Trait-based modeling revealed higher microbial diversity leads to greater ecological resilience in response to an ecosystem disturbance

Jiaze Wang,[1,2]* Victoria J. Coles,[1]* Michael R. Stukel,[3,4] Olivia U. Mason,[3]
[1]Horn Point Laboratory, University of Maryland Center for Environmental Science (UMCES), Post Office Box 775, Cambridge, MD 21613, USA.
[2]School of Earth and Climate Sciences, University of Maine, Orono, ME 04469-5790, USA
[3]Department of Earth, Ocean, and Atmospheric Science, Florida State University, 117 North Woodward Avenue, Tallahassee, FL 32306-4520, USA.
[4]Center for Ocean & Atmospheric Prediction Studies, Florida State University, Tallahassee, FL, USA.

Corresponding author: *Jiaze Wang
Email: jiaze.wang@maine.edu
Corresponding author**:** *Victoria J. Coles
Email: vcoles@umces.edu

Author Contributions: J.W. and V.J.C. designed the research and developed the trait-based model; J.W. investigated and visualized the model results; V.J.C., M.R.S. and O.U.M. supervised and provided feedback on the model performances; O.U.M. provided resources and field data for model comparison; J.W. wrote the paper; V.J.C., M.R.S. and O.U.M. provided reviews and edits.

Competing Interest Statement: Authors declare that they have no competing interests.

Classification: Physical Sciences, Biological Sciences: Microbiology

Keywords: trait-based genomics, microbial community, ocean ecosystem, pulse disturbance, resilience, resistance

This PDF file includes:

Main Text
Figures 1 to 6

Abstract

To quantitatively understand the ecological resilience of an ecosystem with specialized habitats, we focused on deep-sea microbial communities and simulated the response of diverse microbes in specialized habitats to a pulse ecosystem disturbance - the Deepwater Horizon Oil Spill in the Gulf of Mexico. Two microbial communities with equivalent metabolic libraries were acclimated to the presence ("seep-adapted community") or absence ("naïve community") of natural seeps, then their metabolic and ecological responses following the disturbance were compared on both individual and community scales. Higher variability in functional metabolisms in the naïve community without selection pressure created less predictable response to the disturbance. Although spatially and temporally varying degradation rates resulted from the individual complexity of simulated degraders and their interactions with overall community, seep-adapted communities were more efficient in utilizing substrate when spatially averaged. Seep-adapted communities also had more heterogeneous diversity patterns across space and time and presented lower resistance and higher resilience in returning to baseline conditions following the disturbance. The model suggests that communities exposed to transient pulse disturbance or exchanging species with specialized habitats under selection for the disturbance may have greater sustainability in response to disturbance.

Significance Statement

Refugia that differs from ambient conditions are prevalent regionally and foster a diversity of organisms and communities under different selection pressures that may ensure ecosystem productivity and functioning under variable conditions. But their roles in preconditioning ecosystems to disturbances are not well understood. In this study, two Genome-based EmergeNt Ocean Microbial Ecosystems (with and without specialized habitats) were both challenged with a pulse disturbance of a substrate whose uptake was metabolically present in both communities but for which selection pressure only occurred in the specialized habitat. The simulated system-level microbial metabolic functions and microbial community dynamics revealed that specialized refugia provide higher microbial diversity leading to greater ecological resilience and lower ecological resistance in response to a disturbance selected for in the refugia community. Thus, systems with diverse microhabitats may be primed for stability.

Main Text

Introduction

Even oligotrophic habitats that appear homogenous at large spatial scales contain localized heterogeneity in both aquatic and terrestrial environments. These may be physically, or chemically specialized habitats generated by abiotic forces, or biogenic niches created by opportunistic biological activities. After formation, these microhabitats can evolve into biogeochemical hot spots (patches with disproportionately high reaction rates (1)), whose chemical conditions are modulated by microbial communities that are themselves responding to selection pressure from their microenvironment. Their spatiotemporal scales vary from millimeter to kilometer scales and from daily to centuries or more. Such habitats include hydrothermal vent and cold seep habitats in the deep ocean, coral reefs on the continental shelf, ponds in coastal marshes, particles and marine snow aggregates, oil droplets, microplastics, and reduced micro niches within oxic environments, etc. (2–8). Organisms adapted to these biogeochemical hotspots may play critical roles in larger scale ecosystem sustainability and resilience as predicted in the “insurance hypothesis” (9, 10), particularly when the system is perturbed with strong “pulse” disturbances (e.g. oil spills, eutrophic spring freshets or point source nutrient loading) or under shifting “press” conditions (e.g., eutrophication, hypoxia, acidification, climate warming). Essentially, specialized habitats may play a key role in protecting and fostering a diversity of organisms that ensure ecosystem productivity and functioning under variable conditions. However, their priming effects are not yet fully understood and quantified at the system level, due to the complex scales of heterogeneity in a system, to the spatiotemporal challenges of field sampling, and to the difficulty in mimicking extreme environments (e.g., deep-water ecosystems) in the laboratory.

To examine whether specialized habitats impact ecosystem efficiency and timescale of substrate turnover, affect community self-organization and succession in response to pulsed perturbations, and ultimately affect system resilience to a disturbance, we simulated deep-sea microbial communities exposed to the 2010 Deepwater Horizon (DwH) Oil Spill in the Gulf of Mexico (GoM) as a pulse substrate disturbance to the system. Natural seeps in the GoM were hypothesized to act as priming conditions, selecting for microbial communities adapted to hydrocarbon degradation in the simulated system (11–14). We coupled a modified Genome-based EmergeNt Ocean Microbial Ecosystem (GENOME) model to a high resolution physical circulation model (HYCOM). In the model, we established two environmental conditions (seep and no seep) each of which selected for distinct microbial communities in the GoM, then exposed each to a simulated oil spill disturbance. Here, we focus exclusively on processes in the deep hydrocarbon plume which was at >1400m depth. The modified GENOME model includes diverse metabolic functions parameterized based on redox chemistry and randomly allocated to organisms who then form emergent communities. Here, the model is applied to assess adaptation to environmental change due to shifts in the emergent microbial community (19). Moreover, it generates gene and transcript fields which can be compared with observations. The

objectives of this study are to: firstly, quantify the efficiency of the functional metabolisms in the two conditions following the pulse disturbance; secondly, gauge the large-scale ecological responses of the microbial communities to the pulse disturbance; thirdly, explore the role of specialized habitats in priming the ocean ecosystem for future disturbances.

Results and Discussion

Time varying metabolic responses of emergent degraders

In the seep condition, microbes were exposed to low level natural hydrocarbon fluxes within microhabitat niches that slowly exchanged diffusively with the overlying water column prior to the much larger oil spill in early April 2010 (Fig.1(A-F)). In the naïve condition, without this priming effect from seeps, genes for hydrocarbon biodegradation had no utility for organisms prior to the spill. These genes, however, were still expressed at low levels because they co-occurred with other viable metabolisms and the model assumes that the cellular machinery to complete a metabolism cannot be entirely downregulated by an organism. Both simulations, like all biogeochemical models based on organismal concentration, rely on the postulate that "everything is everywhere" within the model domain, such that the response to seep preconditioning is translated throughout the model domain. Thus, this study does not primarily relate to the advection timescales from seep to blowout site in first order. After the pulsed delivery of hydrocarbon substrate, the two conditions yielded different patterns of oil concentrations in the deep plume layer. Dissolved propane and aromatic hydrocarbon trapped in the plume layer were largely degraded by organisms during the disturbance period (Fig.1(B, C, E)). Ethane was also rapidly degraded except that in the no-seep condition it had a secondary maximum concentration at the end of the disturbance and consequently took longer to return to the initial condition (Fig.1(B)), indicating different microbial responses to the disturbance under the two conditions. In contrast, biodegradation of dissolved methane and saturated hydrocarbon occurred primarily after the spill ended (Fig.1(A, D)), although methane degraders began to increase in biomass prior to the peak concentration of methane. Dissolved resins were barely degraded by the organisms, as expected (Fig.1(F)). For the saturated hydrocarbons and resins (Fig. 1(D, F)), the ending background concentrations were higher than the initial conditions in the seep and no-seep conditions by the end of the simulated year, suggesting that the emergent communities established new residual hydrocarbon equilibria relative to the pre-spill conditions that incorporate the residence time of the GOM and the degradation rate. The timescales over which the communities degraded residual hydrocarbons back to the new equilibrium varied between different substrates and their bio-availability and energy density.

The temporal change of hydrocarbon concentrations in the simulated plume layer mainly resulted from the different community composition in each case due to the functional complexity or gene involvement of the individual degraders which shift over time, intrinsically determining the temporally dynamic rate of hydrocarbon uptake (Fig.1(G-R), Fig.S1). For each type of hydrocarbon, there were multiple species in the two emergent communities with metabolisms capable of utilizing each substrate (Fig.1(G-L, M-R)). In general, the seep condition hosted more degraders for each hydrocarbon, exhibiting higher functional diversity (Table.S1). The two simulated communities shared some degraders, as expected, since they both drew from the same pool of organisms. Note that novel organisms were added to the community as conditions drove poorly adapted species below a minimum fractional biomass threshold. According to the gene inventory of the two simulated communities (Fig.S1), some species were single hydrocarbon degraders (e.g., sp8300 and sp2353 in Fig.1(G), sp5813 and sp991 in Fig.1(M)) while others were able to degrade multiple hydrocarbons (e.g., sp5272 in Fig.1(H, I), sp4209 in Fig.1(O, Q)). Species shared across conditions had secondary metabolisms or pathways that supported their growth in the no-seep condition in the absence of hydrocarbons. For example, one methane degrader (sp5813 in Fig.1(G, M)) existed in both experiments, and was able to survive through a light sensitive bacterial nitrification gene (gene: amoA-nl, Fig.S2(A, G)) under both conditions where methane was not a favorable growth strategy.

Differences in genetic potential between microbes determined the individual responses to each substrate at different concentrations. Thus, the genetic potential for a metabolism was not the only constraint to microbial growth under simulated conditions. Some species responded to increasing substrate concentrations with increasing cell densities in both the seep and the no-seep condition (Fig.1(G-L, M-R)). Some organisms had minimal response to the disturbance, suggesting that their growth was largely independent of the hydrocarbon metabolism and its byproducts. For example, the shared ethane degrader sp3344 also consumed nitrogenous dissolved organic matter (Fig.S2(B, H)). Cell densities of species that linearly decreased over the simulation were those that lacked essential genes for growth, that did not have a viable gene complement for survival at depth, or those that had a slower growth rate relative to their loss rate (mortality, grazing, advective or mixing loss in SI Text and Figs.S1-S5). These species would ultimately become extinct.

Identical shared degraders in the two simulated communities also presented different responses to the spilled oil (Fig.1) because other members of the community influenced substrate availability (Fig.1(J-K, P-Q)). Moreover, degraders consuming the same hydrocarbon became active at different times, depending on their alternate metabolisms and substrate uptake thresholds (Fig.1(K, Q)). In the GENOME model, species' interactions within the simulated communities can be directly (e.g., through grazing) and/or indirectly (e.g., through substrate competition) which will also influence the efficiency of substrate uptake by individual degrader. The transcription rates of hydrocarbon-degrading genes were calculated as a function of the uptake rates for substrates which was also co-determined by other substrate limitations. Despite similar pulse disturbance in each simulation, identical degraders yielded different production of transcripts in the two conditions (Figs. 2, S6, S7), indicating differential microbial effort towards hydrocarbon uptake that could only be due to their interactions with other emergent community members. For example, from late June to July, ethane degrader sp1095, which was the most active ethane degrader in the naïve community (no-seep), had lower normalized transcript production of the ethane degrading gene (bmoA-e) than in the seep-adapted community. Meanwhile, nitrate and oxygen at the blow-out site (Fig. 2(E, F)) were more depleted in the no-seep condition from middle June to the end of the oil-spill, which caused the lower ethane-degrading period of degrader sp1095 in that environment. The greater depletion of nitrate and oxygen was caused by other species/degraders in the community who were more active (Materials and Methods). As a result, the no-seep condition ended up having higher ethane concentration (Fig. 1(B), 2(D)) due to less degrading effort, during the period when the well-head was still releasing hydrocarbons.

The community-wide expression of genes or transcripts involved in hydrocarbon biodegradation in the model reflects the integrated biodegradation rate which, with physical processes of mixing and diffusion, shapes the hydrocarbon concentrations on the domain scale (Fig.3). However, even when the two cases shared common active degraders, they did not respond identically to the disturbance because other members of the community influenced substrate availability (Fig.1(J-K, P-Q)). Moreover, degraders consuming the same hydrocarbon became active at different times, depending on their alternate metabolisms and substrate uptake thresholds (Fig.1(K, Q)). Overall, the relative abundance of simulated transcript involved in biodegradation increased and decreased with the concentration of the degradable hydrocarbon under both simulated conditions, except for the resins. The transcript abundance for bmoA-e (ethane, Fig.3(B, H)), bmoA-p (propane, Fig.3(C, I)), and PAH (aromatic hydrocarbon, Fig.3(E, K)) had three phases of change relative to the hydrocarbon release rate. First, the biodegradation rate was lower than the release rate for several days, during which hydrocarbon concentration increased with very little increase in transcript production. After this warm up phase, when the hydrocarbon reached a threshold concentration, the biodegradation rate, as reflected in increasing relative transcript abundance, increased as organismal biomass also increased while the hydrocarbon concentration remained pinned at the threshold level. As the biodegradation rate rose, the more readily utilized ethane and propane began to decline, although the wellhead was still injecting oil. Following the decrease of hydrocarbon concentration, the biodegradation rate dropped to a level comparable to the release rate, after which the remaining hydrocarbons were

gradually degraded. The curve thus illustrated hysteresis in which the initial phases of the spill supported a lagged community response, followed by an acceleration in uptake. Different from other degrading genes, the relative transcript levels for gene pmoA (methane, Fig.3(A, G)) and alkB (saturated hydrocarbon, Fig.3(D, J)) reached their peaks after the spill termination, reflecting preferential community selection for substrates with higher energy yield. This was also seen in the other substrates (ethane, propane, and aromatics) in which there were smaller looping structures reflecting community switching between hydrocarbon metabolisms that allowed the hydrocarbon concentration to increase transiently before becoming energetically favorable again. The extremely small biodegradation rate for the resins in the seep condition declined with its concentration, which was probably due to the availability of other favorable hydrocarbons (Fig.3(F)). The relative transcript level for the resins had no obvious change in the no-seep condition (Fig.3(L)).

Although similar biodegradation phases existed in the naïve community, the relative abundances of transcript in each phase had higher variability than that in the seep-adapted community (Fig.3(B, H), (C, I), (E, K), (F, L)), reflecting less predictable responses of the naïve community when adapting to a wholly novel ensemble of substrates (Fig.2). Different biodegradation rates were intrinsically determined by the different genetic potential of the degraders as well as community composition (Figs. 1(G-R), 2, S1-S7). The concentration threshold for each individual hydrocarbon, at which the biodegradation rate exceeded the release rate, was generally lower in the no-seep condition. This threshold difference was mainly offset by the equilibrium background hydrocarbon concentration in the seep condition (Fig.1(A-F)).

Spatial variations in ecosystem function

The temporal patterns demonstrate how the microbial activities changed with time, but do not show the spatial heterogeneity in the fields. Eddy structures across the Gulf combined with the heterogeneity in distribution of natural seeps create variability in microbial activity in space (Figs. 4, S17). This variability could complicate interpretation of field data from stations sampling different locations in the plume that display spatial differences (20). Spatial patterns have been used as a proxy for the temporal response of microbial activity before and after the disturbance (21), and to derive hydrocarbon biodegradation rates (20, 22). However, heterogeneity in microbial community function or physical transport can result in spatial patterns that do not reflect a simple temporal change in a confined water parcel as demonstrated in decay over time (23). To assess the functional performance of adapted compared with naïve communities, hydrocarbon half-life was computed from a first-order decay model (Fig.4). Differing spatial patterns in community activity resulted from the interactions of microbes with physical advection and diffusion and different hydrocarbon sources in the two simulated conditions. In computing the half-life, biological activity along with physical processes (e.g. mixing and dilution effects) were included to be consistent with field calculations (20). In general, the spatial pattern of the derived half-life follows the pattern of hydrocarbon concentration, and regions with higher concentration have shorter half-lives than the surrounding areas (Fig.4(A-L)). This is consistent with increased microbial hydrocarbon metabolism expressed through upregulation and increased transcript production during high concentrations following the disturbance (Figs. 2-3) when the microbes are released from substrate limitation. However, at times, the relative transcript abundance differs under the same hydrocarbon concentration due to the history of the water parcel, and the biomass of the dominant community members (Figs. 1-3). In other words, nonlinear relationships between biological activities, starting biomass and substrate concentrations contribute to the spatial variability of half-life within a simulated condition. Thus, we observe different regional biodegradation rates or half-lives within simulated conditions and across the two simulated conditions (which have identical physics). These differences mean that hydrocarbon degradation computed from sparse observations are likely to underestimate rates at high substrate concentration, and overestimate rates at low substrate concentrations.

Comparison between the model derived half-lives and available field calculations were drawn for the near field of the wellhead. In the near field (~9 km from the wellhead), the model produces half-lives in the seep (no-seep) condition for all six hydrocarbons are 9.89 ± 6.29 (5.55

± 3.81, methane), 12.90 ± 9.33 (1.85 ± 2.27, ethane), 1.54 ± 1.48 (5.63 ± 3.67, propane), 9.87 ± 6.29 (5.47 ± 3.81, saturated hydrocarbon), 10.87± 8.54 (8.31 ± 5.62, aromatic hydrocarbon), 10.31 ± 6.33 (5.56 ± 3.82, resins) days. The half-lives of n-alkanes (comparable to saturated hydrocarbons in the model) are 1.2-6.1 days (20), according to field and microcosm measurements. Although have a larger range, the half-lives derived from the model overlap with the range from field calculations which also include mixing and dilution effects along with biological activity. Half-lives for biodegradation of aromatic hydrocarbons (C_6-C_{13}, calculated by normalizing the aromatic concentrations with the resin concentrations under the assumption that the resins are mixed and diffused equivalently but little biodegradation occurs) from field data are suggested to be 0.52-1.93 days (22). However, the half-lives from the model are longer than these field data derived calculations. The discrepancy may be due to slow microbial activity resulting from estimating energy yield from the Gibbs free energy of a 'typical' aromatic hydrocarbon, or result from the method of preparing concentration data for half-life derivation. Firstly, as it is shown in Fig.1(F, L, R) and Fig.3(F, L), resins were degraded by the simulated organisms in this model, despite the low activity and concentration. Normalization of hydrocarbon concentration with resins that include any loss terms will create a bias toward much shorter half-lives (Table.S2). Secondly, spatial heterogeneity in hydrocarbon concentrations cannot be neglected because the diffusion of tracers is proportional to the concentration gradient, and different hydrocarbons may have different responses to the same physical diffusion (Figs.S8-13). Detectable resins concentrations are restricted to the wellhead region due to low concentrations, making it challenging to derive half-lives outside of the wellhead region if the resins are used to normalize other hydrocarbons.

To evaluate the net efficiency differences between the naïve and adapted communities, we differenced the half-life estimates on a point-by-point basis. As the local microbial consumption determines the local biodegradation rate, the differences in half-life between the two conditions reflect different regional community efficiency. The high variability in relative abundance of transcripts involved in biodegradation of the naïve community (Fig.3(G-L)), reflects higher variability in community efficiency under the no-seep condition. This creates both negative and positive differences in half-life between the two simulated conditions (Fig.4(M-R)). The positive differences in Fig.4(M-R) reflect shorter half-lives in some regions under the no-seep condition than the seep condition. This is consistent with the result that a higher relative abundance of transcripts at certain hydrocarbon concentrations exist in the naïve community (Fig.3). The regional differences in half-life are dense around zero with negative median values, except for the saturated and aromatic hydrocarbons. Although the half-life differences of saturated hydrocarbon have a positive median value of 0.35 day, the distribution is negatively skewed. The aromatic hydrocarbon has a normal distribution with a median value of zero. The negative median values or the negatively skewed distributions (which either have a more negative range or a higher density at the negative side) mean that the hydrocarbons in the seep condition have shorter half-lives in most regions when spatial heterogeneity is considered. It indicates the seep-adapted community is more efficient than the naïve community in degrading hydrocarbons at regional scale, except for the aromatic hydrocarbon (Fig.4(M-R)).

For the dissolved saturated and aromatic hydrocarbons, the small median values in half-life differences between the two conditions can be explained by the shared active degraders in the two simulations and by the gene complexity of their unique degraders (Fig.3, Fig.S1). For example, degrader sp8210, which only emerged in the seep-adapted community, consumed saturated hydrocarbon when ethane was unavailable (Fig.S3(B)). The two communities, however, still have slight functional differences even with shared active degraders. This could result from competition for substrates or switching of gene functions in one species (Fig.2, Fig.S6). For example, microbe sp4209, as a generalist is able to degrade both propane and aromatic hydrocarbons. It utilized propane first due to its higher concentration and energy yield (Fig.S6(E-E')). However, there were more competitors for propane in the seep-adapted community. The structure of the seep-adapted community was less favorable to the growth of microbe sp4209, which limited its biomass and ultimately constrained its consumption rate for aromatic hydrocarbon. Additionally, in the no-seep simulation, there were more active aromatic degraders

in the naïve community (Fig.1(K, Q), Fig.S2(E, K)), which improved this particular community's performance on aromatic hydrocarbon biodegradation, even without the preconditioning of seep flux. Together these factors explain the wide distribution of half-life differences between the two simulations. Thus, the random allocation of hydrocarbon degrading genes among species can influence the half-life computed from the model slightly, and larger pools of microorganisms or multiple simulations might be needed to address the range of potential outcomes in the future.

Spatial microbial community responses

The community's response to the pulse disturbance included changes in diversity. The background diversity in the seep-adapted community was higher (Simpson's diversity index = ~0.95), while the naïve community had lower diversity between 0.75 and 0.85 before the oil-spill reflecting the smaller number of substrates available and thus the smaller number of potential metabolisms. As was observed in the field (21), microbial diversity decreased near the pulse disturbance relative to that in the uncontaminated deep ocean. In the model, the low diversity region expanded from the wellhead outwards to the oil influenced regions in both simulations (Fig.5), reflecting the additional substrates for novel metabolisms (Figs. S8-S13). Both communities had lower diversity in the disturbed region after the spill ceased, as a result of the dominance of methane degraders (Fig.1(G, M), Fig.3(A, G)). The epicenter or diversity minimum in the seep-adapted community moved away from the wellhead during the spill period, which differed from that in the no-seep condition (Fig.5). The movement of this epicenter was probably due to the fast response to the dispersed oil of an indigenous community which were sustained by hydrocarbons from the surrounding seeps (Fig.5(A-D)). Interestingly, at some deep seep regions (west region of the model domain in Fig.5) the local diversity changed from low to high, and then back to low values, reflecting the adaptation of the seep-adapted community to low levels of local natural seepage, and a fast and different community response to the higher concentrations of dispersed oil. This shift highlights how shifts in the local community structure are sensitive to the concentration of different substrates, not simply their presence and absence. The spatial heterogeneity in seep fluxes, and the difference in seep hydrocarbon composition from the DwH hydrocarbon ratios caused more heterogeneity in the diversity of the seep-adapted community across space and time. The spatial variability in diversity further echoes the challenge in translating spatial patterns in measurements away from the wellhead to a simple linear temporal evolution.

Further measures of resistance and resilience can be used to quantitively evaluate the ecological sustainability of the two different communities. A higher resistance index indicates less change in community diversity, and a higher resilience index indicates faster return to the pre-disturbance diversity level (24–27). The resistance and resilience indices also display spatial variability in the two emerging communities (Fig.6(A-D)). Despite the identical resistance of the two conditions at the wellhead, the seep-adapted community presented lower resistance and higher spatial variability away from the wellhead than the naïve community (Fig.6(A, C, E)). This is consistent with greater heterogeneity in diversity across space and time in the seep condition. The lowest resistance of the seep-adapted community mostly spread across the southern region away from the wellhead, where the diversity decreased from 0.95 to 0.25 (Fig.5(A-D)). However, the naïve community had the lowest resistance around the wellhead and scattering to the south of the wellhead. The positive median or slightly positively skewed distribution of the resilience differences between the two conditions reflects that the seep-adapted community had higher resilience than the naïve community, even around the wellhead where both communities had a relative lower resilience than the surrounding regions (Fig.6(B, D, F)). This reflects that the diversity of the seep-adapted community tended to return faster to its pre-disturbance level, while the change in diversity caused by the disturbance in the naïve community persisted longer. Thus, the preconditioned diverse microbial community responded more rapidly and radically to the pulse disturbance, leading to substantially decreased community diversity, but this rapid response resulted in quick adjustment and recovery.

Ecological implications of the specialized habitats created by seeps

Although community diversity decreased as hydrocarbon increased and degraders became more and more active in both communities, the magnitude of decrease and the timescale for returning to pre-spill conditions varied between scenarios. Adapted to natural seep habitats, the diversity of the indigenous community tended to be more heterogeneous across space and time following the disturbance. The diversity of the seep-adapted community also responded to the pulse disturbance more elastically than the naïve community with greater initial response and faster recovery. However, the differences between the two experiments are likely not within the scope of the limited existing measurements to constrain.

Compared to the naïve community, the seep-adapted community had more species involvement in hydrocarbon biodegradation (Fig.1(G-R) and Table.S1). Biodegradation rates varied nonlinearly with hydrocarbon concentrations in both communities, and the functional performance, as determined by substrate half-life, showed broad spatial heterogeneity in both simulations. While the seep-adapted community generally mediated faster hydrocarbon biodegradation, the naïve community had higher variance in biodegradation than the seep-adapted community at certain hydrocarbon concentrations, as a result of random differences in community structure, gene composition and its allocation within single species and the resultant interactions of these with substrate availability (Fig.2, Fig.S1-S7). Essentially, the naïve community had little selection pressure for hydrocarbon genes, so both low and high concentration hydrocarbon degradation was equally favored. In contrast, the seep adapted community had selection pressure for hydrocarbon degraders that function at low substrate concentration. This explains why in a few restricted regions (i.e., at the wellhead), the naïve community functioned more efficiently as reflected in shorter hydrocarbon half-lives. Despite these restricted regions, the more negatively skewed differences in half-lives demonstrate that the seep-adapted community was more efficient than the naïve community on broad spatial scale. Additionally, the lower variability and higher species involvement in biodegradation indicate that the indigenous community supported by natural seeps gave rise to more orderly and efficient responses to the pulse disturbance due to more species of degraders yielding higher functional redundancy before the disturbance (Table.S1). The responses of the naïve community acclimated to the no-seep condition were less predictable and were reliant on taxa for which hydrocarbon-degradation was a secondary metabolism, since hydrocarbon genes were not selected for prior to the disturbance. Thus, the model predicts that hydrocarbon biodegradation in regions with active seeps, frequent spills, oil drilling, or high rates of hydrocarbon input through shipping for example might have a more stable and predictable hydrocarbon biodegradation response to a disturbance event across a system. Pristine regions without seeps would be less predictable as the natural microbial communities will not be under selection for hydrocarbon degrading genes and hence dependent on stochastic processes associated with advection of hydrocarbon-degrading taxa specialists from other regions or presence of inactive hydrocarbon-degrading genes in generalist species. Extension of this argument to other systems would suggest that specialized habitats can stabilize and create efficiency in pulsed disturbances that are substrate additions.

In a changing ocean, heterogeneous habitats (e.g., natural seeps or marine snow aggregates) culture diverse microbial communities which maintain a range of functions. As the fundamental engineers of life on earth, these microbial communities prime the ocean for different disturbances including pulses of eutrophication, pollution, acidification, hypoxia, and marine heatwaves. Although similar metabolic functions may still exist in naïve communities that are not actively interacting with specialized habitats, the indigenous communities associated with specialized habitats tend to have higher functional redundancy and are more efficient in response to disturbances at broad spatial scales. Additionally, the diversity of the indigenous community with preconditioning has a more elastic response to disturbances, which maintains the stability of the microbial ecosystem. However, due to the heterogeneity of ocean habitats and the variability in dispersal timescales, field observations at different locations and times may reflect responses of adapted communities or of naïve communities, or even of both. It is vital to explore the diverse

microbial functions in specialized habitats, and to take the spatiotemporal heterogeneity of the ocean into consideration when the community response to pulse disturbances is investigated.

Materials and Methods

Hydrocarbon pulse disturbance

Although hydrocarbons released at the Macondo well (wellhead location: 88.39ºW and 28.74 ºN) include a wide variety of soluble and insoluble hydrocarbon compounds at certain temperature and pressure conditions (28), only the dissolved hydrocarbon portion is considered to influence the system at the surface and deep water (deep water plume layer; ~1000-1600m) in this model. Considering the two main phases (gas and oil) and the compositions of the spilled hydrocarbons, the dissolved hydrocarbons are grouped into 6 hydrocarbons in the model, including methane, ethane, propane, saturated hydrocarbons, aromatic hydrocarbons and resins. Each group has a typical molecular formula in order to convert them from mass to mole units. The mass fraction of each group (Table.S4) is from multiple data sources (17, 18, 21, 28), and is converted into moles of hydrocarbon per second for the model. These hydrocarbons are input to the model from April 20th to July 15th, 2010 at the Macondo well site, and a final mole concentration per second for each group is derived from their mole input rate and the volume of a grid cell in the plume layer at the oil-spill site. Given the horizontal and vertical resolution of the HYCOM configuration (~9 km in horizontal, and hundreds of meters thickness in vertical at deep water), the grid cell volume at the oil-spill site is too large to give reasonable mole concentrations for each hydrocarbon group released when compared with the field measurements. However, the absolute concentration rather than the substrate flux dictates the microbial substrate limitation and thus growth rate. Therefore, we adapted the input rate of the hydrocarbon pulse disturbance to be 5-fold larger in this model in order to simulate hydrocarbon concentrations within a model cell consistent with observations. This means that the gross magnitude of the oil spill, and its fate in the environment would have larger impact in the model than observations.

Typical formulas in Table S4 are derived from the observed dissolved concentrations of different hydrocarbons in each group (i.e. the aromatic hydrocarbon group includes benzene, toluene, xylene, etc.) (17, 18, 21, 28). In a series of redox reactions, a typical formula for a group of hydrocarbons can be derived by keeping the conservation of total carbons involved in the reactions and/or total electrons donated by all hydrocarbons in the group of hydrocarbons. Because hydrocarbons are energy and carbon sources for the organisms in the GENOME model, the Gibbs free energy of each hydrocarbon group is needed to compute the biomass yield on each group. Given the limited availability of the Gibbs free energy of each typical formula, conservation of donated electrons is applied to derive the typical formulas and the mass fractions to the total dissolved spilled oil. The exception is the resins group which represents the heavy oil component in the spilled oil and is considered to be insoluble in most cases. Given limited field measurements of the dissolved heavy oil, the typical formula of the resins is set to $C_{30}H_{52}$ (29), which is a type of heavy oil deposited on the seafloor. Although these typical formulas and their derived concentrations are based on electron conservation, the total amount of carbons involved in redox reactions are not very different from those with carbon and electron conservation. It needs to be noted that the typical formula for each hydrocarbon group is based on the chemical composition of the DwH oil-spill and is only appropriate for this case.

The Gibbs free energy for the aerobic oxidation of the typical hydrocarbons at the appropriate deep-water thermodynamic condition (at temperature of 278.15 kelvin and pressure of 12 Mpa) are calculated using the CHNOSZ library for the software package R. All related redox reactions of hydrocarbons are listed below:

$$CH_4 + 2O_2 \rightarrow CO_2 + 2H_2O$$

$$\frac{1}{2}C_2H_6 + \frac{7}{4}O_2 \rightarrow CO_2 + \frac{3}{2}H_2O$$

$$\frac{1}{3}C_3H_8 + \frac{5}{3}O_2 \rightarrow CO_2 + \frac{4}{3}H_2O$$

$$\frac{1}{10}C_{10}H_{22} + \frac{31}{20}O_2 \rightarrow CO_2 + \frac{11}{10}H_2O$$

$$\frac{1}{7}C_7H_8 + \frac{9}{7}O_2 \rightarrow CO_2 + \frac{4}{7}H_2O$$

$$\frac{1}{30}C_{30}H_{52} + \frac{43}{30}O_2 \rightarrow CO_2 + \frac{13}{15}H_2O$$

Model experimental design

To investigate the role of natural seeps in preconditioning the microbial system for massive hydrocarbon pulse disturbance, two model communities are constructed under environmental conditions with and without natural seeps. In the natural seep experiment, dissolved hydrocarbons from natural seepages are grouped into the same six types as the spilled oil from the Macondo well, and are released at given rates from 938 natural seep sites (11). Their mass release rates (Table.S5) are derived from an annual mass flux (30), and their mass fractions are estimated from field observations in the open ocean (31–33). In the simulation without natural seep flux, the six hydrocarbons are set to zero concentration prior to the oil spill. Up to 17 substrates and 58 microbial species coexist in this model system. For each case, the model community adapts to the Gulf of Mexico during a "spin-up" period through the replacement of organisms whose biomass is below 1% of the community everywhere in the model with new organisms drawn from the same organism pool. This pool is constructed from the gene library (Table.S3) (19). Over time, organisms adapted to the local environment emerge to develop community structures that utilize the available resources (Fig.S1). To investigate the dynamics of the two community structures differentiated solely by the seep vs no-seep conditions and exposed to the massive hydrocarbon disturbance of the Deepwater Horizon Oil Spill, organism replacement is terminated at the beginning of year 2010, prior to the spill in the two model experiments.

Acknowledgments

We would like to thank Erick Olvera-Prado and Alexandra Bozec for model setting up on High Performance Computation cluster at Florida State University. This research was made possible by a grant from the Gulf of Mexico Research Initiative. Gulf of Mexico Research Initiative Grant Year 8-10 Research Grants (RFP-VI) (EC, VJC, DD, CH, RH, TJHSU, AM, OM, SM, MS, KT). The finalization of this work was supported by the DOE Office of Science Early Career Research program as part of research in Earth System Model Development within the Earth and Environmental System Modeling Program. We would also like to show our gratitude to Dr. Benjamin N. Sulman from the Oak Ridge National Laboratory (ORNL), who is the lead PI of the DOE sponsored Early Career Award, for his valuable comments and support in finalizing this research. We also thank the ORNL and the Climate Change Science Institute at ORNL for providing resources during the finalization process. ORNL is managed by UT-Battelle, LLC, under contract DE-AC05-00OR22725 with the US Department of Energy (DOE).

References

1. M. E. McClain, *et al.*, Biogeochemical Hot Spots and Hot Moments at the Interface of Terrestrial and Aquatic Ecosystems. *Ecosystems* **6**, 301–312 (2003).
2. D. Bianchi, T. S. Weber, R. Kiko, C. Deutsch, *Global niche of marine anaerobic metabolisms expanded by particle microenvironments* (2018) https:/doi.org/10.1038/s41561-018-0081-0.
3. M. J. Eichner, *et al.*, Chemical microenvironments and single-cell carbon and nitrogen uptake in field-collected colonies of Trichodesmium under different pCO2. *ISME J.* **11**, 1305–1317 (2017).
4. B. B. Jørgensen, Bacterial sulfate reduction within reduced microniches of oxidized marine sediments. *Mar. Biol.* **41**, 7–17 (1977).
5. M. Kühl, R. N. Glud, H. Ploug, N. B. Ramsing, Photosynthesis-Coupled Respiration in an.

J. Phycol. **32**, 799–812 (1996).
6. H. Ploug, Small-scale oxygen fluxes and remineralization in sinking aggregates. *Limnol. Oceanogr.* **46**, 1624–1631 (2001).
7. H. Ploug, M. Kühl, B. Buchholz-Cleven, B. B. Jørgensen, Anoxic aggregates - An ephemeral phenomenon in the pelagic environment? *Aquat. Microb. Ecol.* **13**, 285–294 (1997).
8. A. L. Shanks, J. D. Trent, Marine snow: Microscale nutrient patches. *Limnol. Oceanogr.* **24**, 850–854 (1979).
9. S. Naeem, S. Li, Biodiversity enhances ecosystem reliability. **390**, 507–509 (1997).
10. S. Yachi, M. Loreau, Biodiversity and ecosystem productivity in a fluctuating environment: The insurance hypothesis. *Proc. Natl. Acad. Sci. U. S. A.* **96**, 1463–1468 (1999).
11. I. R. MacDonald, *et al.*, Natural and unnatural oil slicks in the Gulf of Mexico. *J. Geophys. Res. Ocean.* **120**, 8364–8380 (2015).
12. E. B. Overton, *et al.*, Chemical composition of macondo and other crude oils and compositional alterations during oil spills. *Oceanography* **29**, 50–63 (2016).
13. H. C. (ed. . Ward, *Water quality of the Gulf of Mexico* (2017).
14. K. A. Kvenvolden, C. K. Cooper, Natural seepage of crude oil into the marine environment. *Geo-Marine Lett.* **23**, 140–146 (2003).
15. R. Lamendella, *et al.*, Assessment of the deepwater horizon oil spill impact on gulf coast microbial communities. *Front. Microbiol.* **5**, 1–13 (2014).
16. C. M. Reddy, *et al.*, Composition and fate of gas and oil released to the water column during the Deepwater Horizon oil spill. *Proc. Natl. Acad. Sci. U. S. A.* **109**, 20229–20234 (2012).
17. D. L. Valentine, *et al.*, Propane respiration jump-starts microbial response to a deep oil spill. *Science (80-.).* **330**, 208–211 (2010).
18. A. R. Diercks, *et al.*, Characterization of subsurface polycyclic aromatic hydrocarbons at the Deepwater Horizon site. *Geophys. Res. Lett.* **37**, 1–6 (2010).
19. V. J. Coles, *et al.*, Ocean biogeochemistry modeled with emergent trait-based genomics. *Science (80-.).* **358**, 1149–1154 (2017).
20. T. C. Hazen, *et al.*, Deep-sea oil plume enriches indigenous oil-degrading bacteria. *Science (80-.).* **330**, 204–208 (2010).
21. O. U. Mason, *et al.*, Metagenome, metatranscriptome and single-cell sequencing reveal microbial response to Deepwater Horizon oil spill. *ISME J.* **6**, 1715–1727 (2012).
22. A. E. Thessen, E. W. North, Calculating in situ degradation rates of hydrocarbon compounds in deep waters of the Gulf of Mexico. *Mar. Pollut. Bull.* **122**, 77–84 (2017).
23. D. L. Valentine, *et al.*, Dynamic autoinoculation and the microbial ecology of a deep water hydrocarbon irruption. *Proc. Natl. Acad. Sci. U. S. A.* **109**, 20286–20291 (2012).
24. A. Shade, *et al.*, Fundamentals of microbial community resistance and resilience. *Front. Microbiol.* **3**, 1–19 (2012).
25. K. N. Suding, K. L. Gross, G. R. Houseman, Alternative states and positive feedbacks in restoration ecology. *Trends Ecol. Evol.* **19**, 46–53 (2004).
26. D. A. Orwin, K.H., Wardle, New indices for quantifying the resistance and resilience of soil biota to exogenous disturbances. *Soil Biol. Biochem.* **36**, 1907–1912 (2004).
27. W. E. Westman, Measuring the Inertia and Resilience of Ecosystems. *Bioscience* **28**, 705–710 (1978).
28. C. M. Reddy, *et al.*, Composition and fate of gas and oil released to the water column during the Deepwater Horizon oil spill. *Proc. Natl. Acad. Sci.* **109**, 20229 LP – 20234 (2012).
29. D. L. Valentine, *et al.*, Fallout plume of submerged oil from Deepwater Horizon. *Proc. Natl. Acad. Sci. U. S. A.* **111**, 15906–15911 (2014).
30. Coleman, J., Baker, C., Cooper, C.K., Fingas, M., Hunt, G., Kvenvolden, K.A., Michel, K., Michel, J., R. B. McDowell, J., Phinney, P., Rabalais, N., Roesner, L., Spies, *Oil in the Sea III* (The National Academies Press, 2003) https:/doi.org/10.17226/10388.
31. L. M. Sauer, T.C., Jr., Sackett, W.M. and Jeffrey, Volatile liquid hydrocarbons in the

surface coastal waters of the Gulf of Mexico. *Mar. Chem.* **7**, 1–16 (1978).
32. T. L. Wade, M. C. Kennicutt, J. M. Brooks, Gulf of Mexico Hydrocarbon Seep Communities: Part III. Aromatic Hydrocarbon Concentrations in Organisms, Sediments and Water. *Mar. Environ. Res.* **27**, 19–30 (1989).
33. T. Mitra, Siddhartha, Bianchi, A preliminary assessment of polycyclic aromatic hydrocarbon distributions in the lower Mississippi River and Gulf of Mexico. *Mar. Chem.* **82**, 273–288 (2003).

Figures

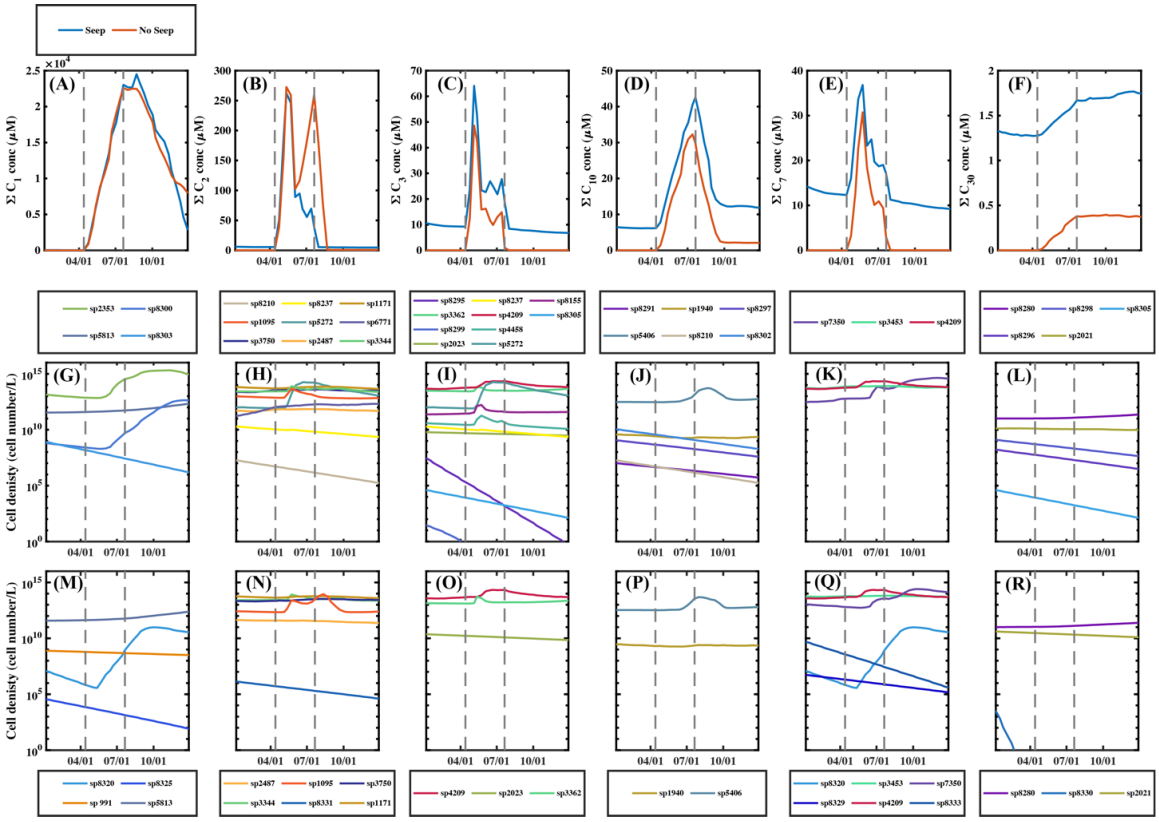

Figure 1. The responses of hydrocarbon degraders in seep-adapted and naive emergent communities to the spilled oil. Spatially integrated dissolved hydrocarbon concentrations in the plume layer: **(A)** methane, **(B)** ethane, **(C)** propane, **(D)** saturated hydrocarbon, **(E)** aromatic hydrocarbon, **(F)** resins. Cell density of different hydrocarbon degraders in the seep condition: **(G)** methane degraders, **(H)** ethane degraders, **(I)** propane degraders, **(J)** saturated degraders, **(K)** aromatic degraders, **(L)** resins degraders. Cell density of different hydrocarbon degraders in the no-seep condition: **(M)** methane degraders, **(N)** ethane degraders, **(O)** propane degraders, **(P)** saturated degraders, **(Q)** aromatic degraders, **(R)** resins degraders. The two dashed grey lines represent the initiation and termination of the oil-spill; different line colors represent different species, which are marked with a numeric ID from the predetermined microbial pool (e.g., sp5813). (In this model, hydrocarbon degraders are defined as microbes that carry genes for degrading each hydrocarbon. Time series of their cell densities and the hydrocarbon concentrations are calculated by integrating over each grid cell in the plume layer over the whole model domain. Note: the y axis is logarithmic).

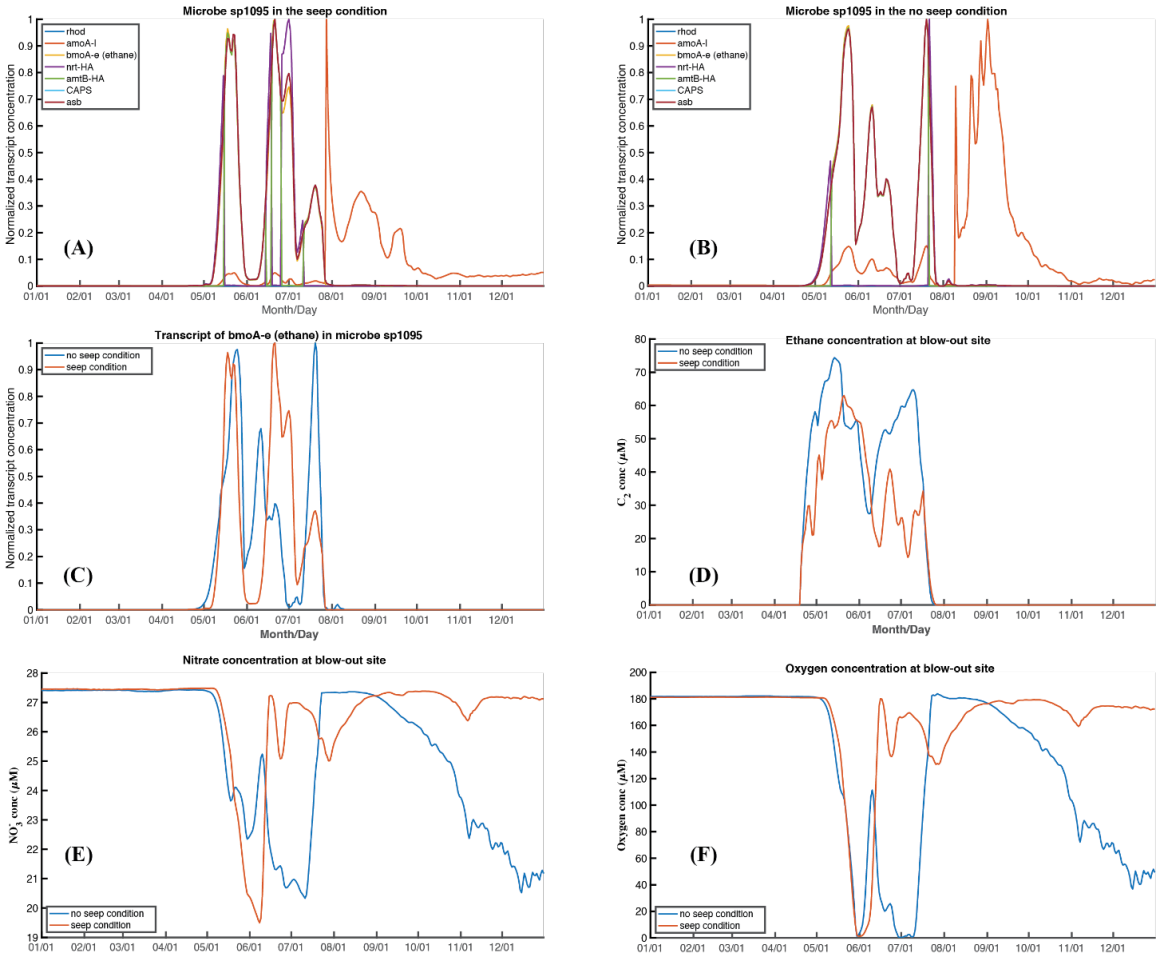

Figure 2. Example of microbial effort (shared degrader sp1095) and substrate availability (ethane, nitrate, and oxygen) in the plume layer at the blow-out site. Normalized transcripts of all genes in degrader sp1095 **(A)** in the seep-adapted community and **(B)** in the naïve community. Comparison of biogeochemistry between the seep condition and no-seep condition in normalized transcript level of gene **(C)** bomA-e (degrading ethane), **(D)** ethane concentration, **(E)** nitrate concentration, and **(F)** oxygen concentration.

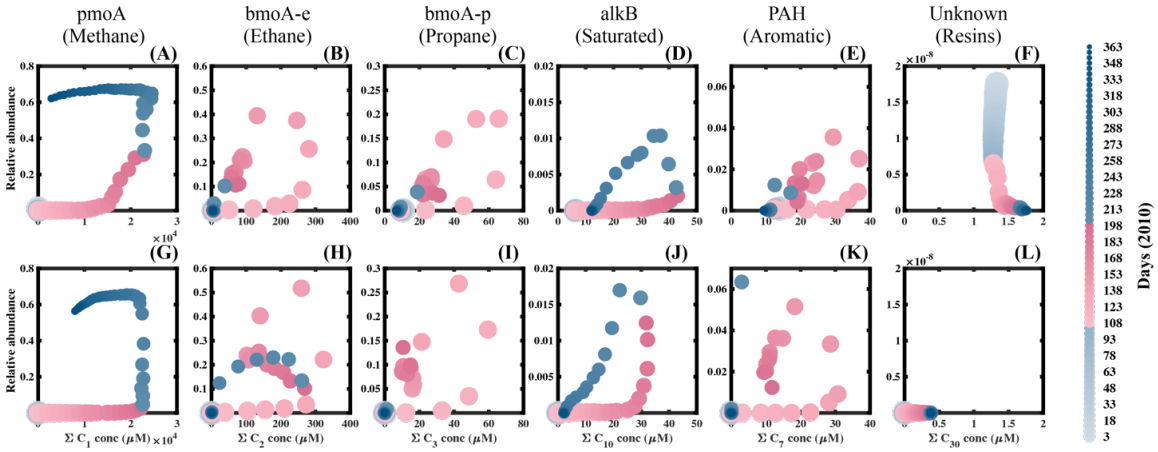

Figure 3. Community-wide gene involvement in hydrocarbon degradation in the simulated transcript data. pmoA, methane degrading gene expression as a function of methane concentration: (A) in the seep condition and (G) in the no-seep condition; bmoA-e, ethane degrading gene expression as a function of ethane concentration: (B) in the seep condition and (H) in the no-seep condition; bmoA-p, propane degrading gene expression as a function of propane concentration: (C) in the seep condition and (I) in the no-seep condition; alkB, saturated degrading gene expression as a function of ethane concentration: (D) in the seep condition and (J) in the no-seep condition; PAH, aromatic degrading gene expression as a function of ethane concentration: (E) in the seep condition and (K) in the no-seep condition; Unknown gene for resins degrading gene expression as a function of ethane concentration: (F) in the seep condition and (L) in the no-seep condition. Note: pink colors represent the time period of the perturbation with a 5-day interval; each subplot has different y-axis and x-axis scale.

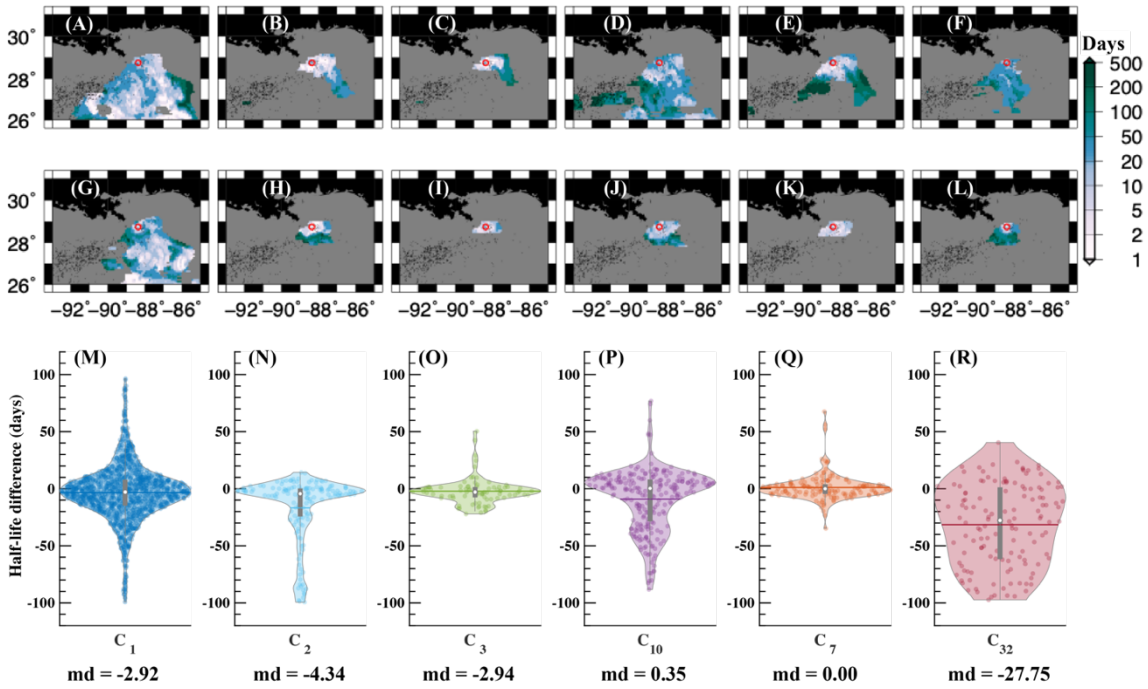

Figure 4. Derived half-lives for dissolved hydrocarbons in two simulated conditions. Natural seep condition: (A) methane, (B) ethane, (C) propane, (D) saturated hydrocarbon, (E) aromatic hydrocarbon, and (F) resins. NO seep condition: (G) methane, (H) ethane, (I) propane, (J) saturated hydrocarbon, (K) aromatic hydrocarbon, and (L) resins. Half-life differences between the seep condition and no-seep condition for (M) methane, (N) ethane, (O) propane, (P) saturated hydrocarbon, (Q) aromatic hydrocarbon, and (R) resins. (Note: Red circle represents the well head location; white dots in violin plots indicate median values (md), and horizontal lines indicate mean values. The negative half-life differences mean that the half-life in the seep condition is shorter than that in the no-seep condition, and md represents median value. The regions of half-life are different among hydrocarbons in the two simulations because a fitting curve is valid when the residual standard error is smaller than 0.25, and please refer to the estimation of half-life in the analysis methods section in SI Text. The differences were calculated only for shared locations).

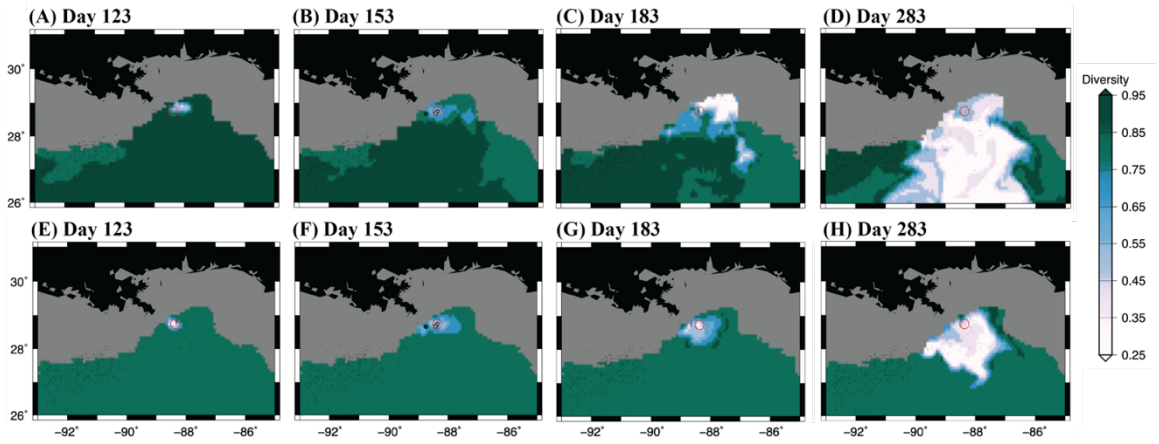

Figure 5. The response of community diversity at different days of year 2010 in the deep plume layer. Simpson's diversity for the communities (A-D) in the seep condition and (E-H) in the no-seep condition. Note: Red circle represents the well head location; colorful circles in (B) at day 153 represent field sampling sites after (21), and the field data color scale is the same as the map color scale. The oil-spill happened at day 110 of year 2010. The field sampling date is 10 days before or after the selected mapping date. Small black dots represent seep locations.

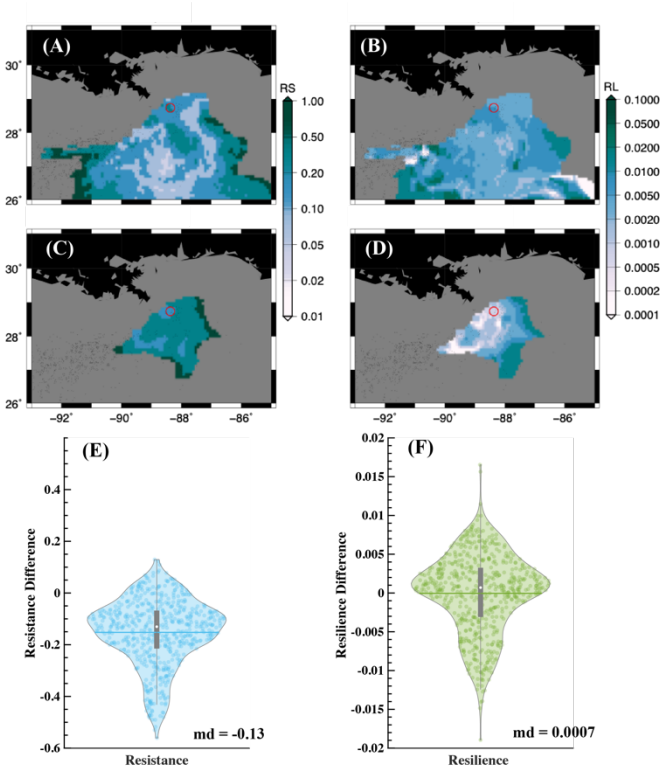

Figure 6. Diversity-derived spatially explicit resistance and resilience indices for the two simulated conditions. RS: resistance index (A) in the seep condition and (C) in the no-seep condition; RL: resilience index (B) in the seep condition and (D) in the no-seep condition. Spatially composited differences for (E) the resistance index and (F) resilience index between the seep condition and the no seep condition. (Note: red circles in spatial maps represent the wellhead location; white dots in the violin plots represent the median values (md), and horizontal lines represent the mean values. The negative differences mean indices in the seep condition are smaller than those in the no seep condition. The regions that the two indices are evaluated over are different in the two simulations because changes in diversity less than 20% of the pre-disturbance level are masked out, please refer to resistance and resilience metrics in the analysis methods section in SI Text).

Supporting Information for

Trait-based modeling revealed higher microbial diversity leads to greater ecological resilience in response to an ecosystem disturbance

Jiaze Wang*, Victoria J. Coles*, Michael R. Stukel, Olivia U. Mason

Corresponding author: Jiaze Wang
Email: jiaze.wang@maine.edu

Corresponding author: Victoria J. Coles
Email: vcoles@umces.edu

This PDF file includes:

Supporting text
Figures S1 to S24
Tables S1 to S5
SI References

Supporting Information Text

Physical model

The ocean circulation model used is the Hybrid Coordinate Ocean Model (HYCOM; http://www.hycom.org). The regional HYCOM Gulf of Mexico configuration is run with horizontal resolution of 0.08º or ~9 km in the domain from 18.9ºN to 31.96ºN and from 98ºW to 76.4ºW. A total of 20 hybrid layers are used for the vertical grid. Sponge layers are incorporated at the southeastern boundary in the model, and nitrate, oxygen, temperature, salinity, and layer thickness are relaxed to climatological values along these boundaries. River runoff along the GoM coast is from a monthly climatology, with inputs of sediment, nitrate, ammonium, organic matter, and organic carbon (1–4). Atmospheric forcing is from hourly fields of the Climate Forecast System Reanalysis (CFSR) from 1992 to 2010 (5).

Ecosystem Model development

In the GENOME model, each organism is randomly assigned a size that dictates basic functional relationships of growth rate, uptake kinetics and sinking rate using allometric theory. Then, organisms are randomly assigned a number of functional "genes" from a predetermined gene library of metabolic functions (6) (note that one model "gene" actually represents all of the genes necessary for a specific metabolic process). At the same time, costs and benefits associated with each gene are superimposed to determine the organism's final environmental responses. In the end, an artificial microbial community which can respond to environmental substrates and conditions such as oil or light is built. Finally, these organisms are introduced into the physical model. If one organism dies out, it will be replaced by a new one to get a broad diversity of microbes in the community (7).

Beginning with the ecosystem model framework introduced above, the GENOME model has been modified to increase its flexibility and adaptability, by including metabolic functions related to the uptake of energy substrates. New genes that are related to hydrocarbon degradation and temperature dependance have been added to the existing genome library for the GENOME model (7) (Table.S3). Each modeled microbe is randomly assigned several genes (< 7 genes) from the predetermined genome library which superimpose costs and benefits to the organism's growth. The more genes an organism carries, the higher net costs it carries. Details of this modeling approach are described in (7), but one major alteration here is that the energy provided by substrates taken up by organisms which contribute to their growth is derived from the relationship between organisms' growth yield (Y_c, carbon mole (mole electron donor)$^{-1}$)) and the energy yield (ΔG_{e^-}, kilojoules (mole electron donor)$^{-1}$) of related redox reactions at certain temperature and pressure conditions (Eq.1) (8),

$$Y_c = \frac{(2.08 - 0.0211 \Delta G_{e^-})}{24.6} \quad \text{(Eq.1)}$$

The molecular weight of the microbial biomass is 24.6 $g\ (mol\ C)^{-1}$ which is derived from the generic microbial biomass formula of $CH_{1.8}O_{0.5}N_{0.2}$ (9), and ΔG_{e^-} is calculated using Eq.2.

$$\Delta G = \Delta G_0 + RT \ln Q = \Upsilon_{e^-} \times \Delta G_{e^-} \quad \text{(Eq.2)}$$

ΔG is the change of the Gibbs free energy in a redox reaction with unit of kJ/rxn (kJ per reaction), and it is related to the stoichiometric coefficients in the reaction. ΔG_0 with unit of kJ/rxn is the change of the Gibbs free energy in the redox reaction under standard conditions (at 1 bar pressure and the specified temperature of 298.15 k or 25 °C). T is temperature (kelvin). Q is the reaction quotient (unitless), and R is the gas constant (kilojoules/kelvin/mole). Υ_{e^-} is the stoichiometric coefficient of the electron donor (ED) in a redox reaction.

Because nitrogen units are used in the GENOME model, the growth yield Y_c is converted from carbon unit to nitrogen unit with the Redfield ratio (C:N = 106:16, mol:mol) for consistency, which is based on the Eq.3.

$$Y_N = Y_c \frac{106}{16} \quad \text{(Eq.3)}$$

Analysis methods

Cell density

Each microbe is treated as a prolate spheroid volume (PSV, μm^3) with a length (L, μm) and a breadth (B, μm) (Eq.4, (10)). Relationships between nitrogen per cell (NPC, pgN/m^3) and cell volume are applied to derive the cell density, or the number of cells per cubic meter for each species from the nitrogen-based biomass simulated in the model (Eq.5-6, (11–13)).

$$PSV = \frac{\pi}{6} LB^2 \quad \text{(Eq.4)}$$

$$\left(where\ L = D, B = \frac{D}{2}, D\ is\ the\ diameter\ of\ an\ organism, \mu m\right)$$

$$NPC = 0.024PSV \qquad (PSV \leq 180 \mu m^3) \quad \text{(Eq.5)}$$

$$NPC = 0.032PSV^{0.939} \quad (PSV > 180\ \mu m^3) \quad \text{(Eq.6)}$$

Resistance and resilience metrics

Community responses to the pulse disturbance are represented by Simpson's Diversity Index. Community stability in microbial ecology, defined by (14), is comprised of two quantifiable metrics which are resistance and resilience (15). To compare the disturbance responses of the two simulated communities, the two metrics of community stability are investigated in terms of a compositional parameter which is Simpson's Diversity index in this context (Eq.7-8, (15–18)). Here, resistance (RS) reflects the magnitude of change in the diversity index (the lower the value, the larger the change), and resilience (RL) reflects the rate of return to the pre-disturbance level of diversity after a lag period (the higher the value, the faster the return).

$$RS = 1 - \frac{2|D_0 - D_L|}{D_0 + |D_0 - D_L|} \quad \text{(Eq.7)}$$

$$RL = \left[\frac{2|D_0 - D_L|}{|D_0 - D_L| + |D_0 - D_n|} - 1\right] \div (t_n - t_L) \quad \text{(Eq.8)}$$

D_0 is the mean diversity before disturbance, D_L is the diversity at time t_L when the maximum change in diversity happens, and D_n is the diversity level at time t_n, which is at the end of year 2010 in this study. Changes in diversity less than 20% of the pre-disturbance level are neglected.

Estimation of biodegradation kinetics and half-life

First-order kinetics (κ), which is also referred as first-order decay constant or biodegradation rate constant, is normally applied implicitly in studies about the biodegradability of hydrocarbons (Eq.9, (19–22)). The biodegradation half-life ($t_{1/2}$), the time for half of a hydrocarbon in the system to be degraded, is obtained by Eq.10.

$$C_t = C_0 e^{-\kappa t} \quad \text{(Eq.9)}$$

$$t_{1/2} = \frac{\ln 2}{\kappa} \quad \text{(Eq.10)}$$

In the above two equations, C_0 is the initial concentration (μM), C_t is the residual concentration (μM) at time t, κ is the decay constant (day^{-1}), t is time (day), and $t_{1/2}$ is biodegradation half-life (day).

To obtain a spatial map of half-lives for each type of hydrocarbon simulated for comparison with observations, an exponential decay curve with at least three values is fitted to the change of hydrocarbon concentration over time at each grid point. The greatest hydrocarbon concentration obtained after the oil-spill happened is considered as the initial concentration at each location, and the lowest threshold of 0.001 μM is applied for this maximum value to distinguish a significant hydrocarbon increase from the background concentration. Package nlsLM from library minpack.lm in R is used to fit the exponential curve (Eq.9). A fitting curve is considered to be valid when the residual standard error is smaller than 0.25. The decay constants (κ) and half-lives ($t_{1/2}$) are then estimated for locations with valid fitting curves.

Model validation and performance

Hydrocarbon concentrations in the plume layer

To obtain simulated hydrocarbon concentrations comparable to the observed field values, the quantity of the released hydrocarbons in the model are 5-fold larger than the actual spilled mass. Except for methane (Fig. S8) which is much higher than the observed values in some regions, the simulated hydrocarbon concentrations are comparable to the observed field values (Figs. S9-13). As observed, the spilled hydrocarbons in the model disperse from the wellhead through diffusion and advection in deep water, and the majority of spilled oil stays in the deep plume layer. The methane concentrations within 18-km range of the wellhead vary between 0-1653 μM during the oil spill period, with a regional mean concentration between 0-362.700 μM. The concentration of ethane around the wellhead ranges from 0 to 61.680 μM, with a regional mean value varying among 0-9.921 μM. The propane concentration during the oil spill period is from 0 to 15.920 μM, with a regional mean concentration around 0-1.991 μM. For the saturated hydrocarbon, the regional concentration is between 0-2.788 μM, with a regional mean concentration varying from 0 to 0.6111 μM. The aromatic hydrocarbon around the wellhead region has concentration between 0 and 5.441 μM, with a regional mean concentration around 0-0.9433 μM. Considering that the physical model is not data assimilative, nor high enough resolution to resolve the detailed flow at the wellhead, the simulated oil spill performs reasonably well in the model. Here, the objective of this study is to investigate whether an indigenous community cultured by natural seeps outperforms a naïve community in a no-seep environment under the same pulse disturbance. Thus, the specifics of the eddy dynamics need not be exact. The elevated methane concentrations in the two model experiments are at the same level (Fig. S8), which means that the comparison between two experiments is valid, and that the methane biodegradation in the model may be slower than observed. The observed field concentrations (6, 22, 23) are grouped into the six types of hydrocarbons using the same method as in the model.

Oxygen and dissolved nitrogen concentrations in the plume layer

Simulated oxygen and nitrate concentrations also match the field observations (24) (Figs.S14-15). Depletions of oxygen and nitrate initiate around the wellhead, and spread out with the dispersed oil, which indicates strong spatiotemporal variability. Oxygen and nitrate are much more depleted in heavily oiled regions, especially around the wellhead location. Following the released oil, the oxygen concentration within 18-km range around the wellhead decreases from 186.900 to 1.302 μM, with a regional mean concentration varying from 181.400-88.620 μM. The nitrate concentration around the wellhead decreases from 28.000 to 18.010 μM, with a regional mean concentration ranging between 23.940 and 27.450 μM. Ammonium concentration also agrees closely with the field observations (23) (Fig.S16), and the elevated ammonium concentration follows the released oil. The ammonium concentration around the wellhead increases from 0 to 3.338 μM, with a regional mean value ranging from 0 to 0.932 μM during the oil spill period.

Emergent communities and metabolisms in the plume layer

The biomass of hydrocarbon degraders in the model, represented by the density of cells (cells per liter), increases with the released oil. The increase is about two orders of magnitude in the heavily oiled region from ~10^9 to ~10^{11} cells per liter at day 153 of 2010 (Fig.S17), which increase is similar to the observed increase in the field from ~10^6 to ~10^8 cells per liter (6). Higher cell concentrations in the model compared with observations may suggest that the model has higher substrate availability or lower mortality than the mesopelagic ocean. The emergent community also shows lower Simpson's diversity following the dispersed oil (Fig.5), consistent with observations at proximal and distal stations (6). Furthermore, the gene concentrations involved in hydrocarbon degradation also increase as they are observed in the field (Figs S18-23, (6)).

Responses of individual species to the oil-spill

In the GENOME model, the responses of individual species to the oil disturbance were initially driven by its functional complexity (Fig. S1). Some individual degraders responded to the spilled oil with increasing biomass (represented by cell densities) as it was expected. While other degraders either responded to the oil disturbance with decreasing biomass or had no response (Figs. S2, S4). For example, propane degrader sp8295 and saturated alkane degrader sp8297 lacked genes that were related to nitrogen acquisition for their growth, so their growth was inhibited, and they were gradually lost from the system (Figs. S2(C-D), S4(A)). For propane degrader sp8299 in the seep-adapted community and methane degrader sp8325 in the naïve community, the lack of gene CAPs for adaptation to low temperature (psychrophile) greatly inhibited their performance in the deep plume relative to the surface water (Figs. S1(B), S4(C, G), S5). In contrast, other degraders who also lacked the gene CAPs but had only modest change of cell densities in deep water, corresponded to those that had the gene for shell formation and commensurate increased cell sinking rates (named as sil in the model; e.g., sp2487, Figs. S4(B, H), S7) resulting in their steady resupply from surface layers. However, for degraders sp8210 and sp8295 in the seep-adapted community, and degraders sp8333 and sp8330 in the naïve community, their decreases in cell densities were due to inefficient/slow growth compared to mortality, grazing, and/or sinking, despite their adaptation to the low temperatures in the deep water (Figs. S2(C, D, K, L), S3).

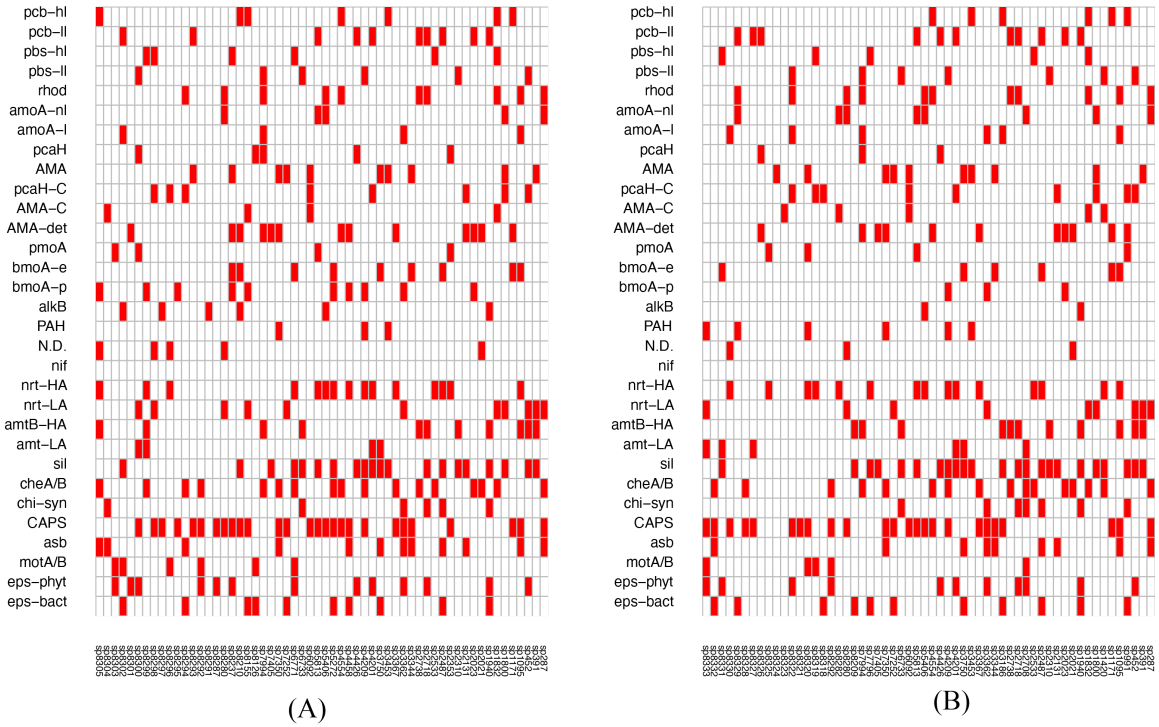

Fig. S1. The genome of simulated microbial community. (A) the seep-adapted community. (B) the naïve (No-seep) community. Gene names are listed on the left-hand side whose functions in the model are explained in Table S3, and microbial species IDs are listed at the bottom.

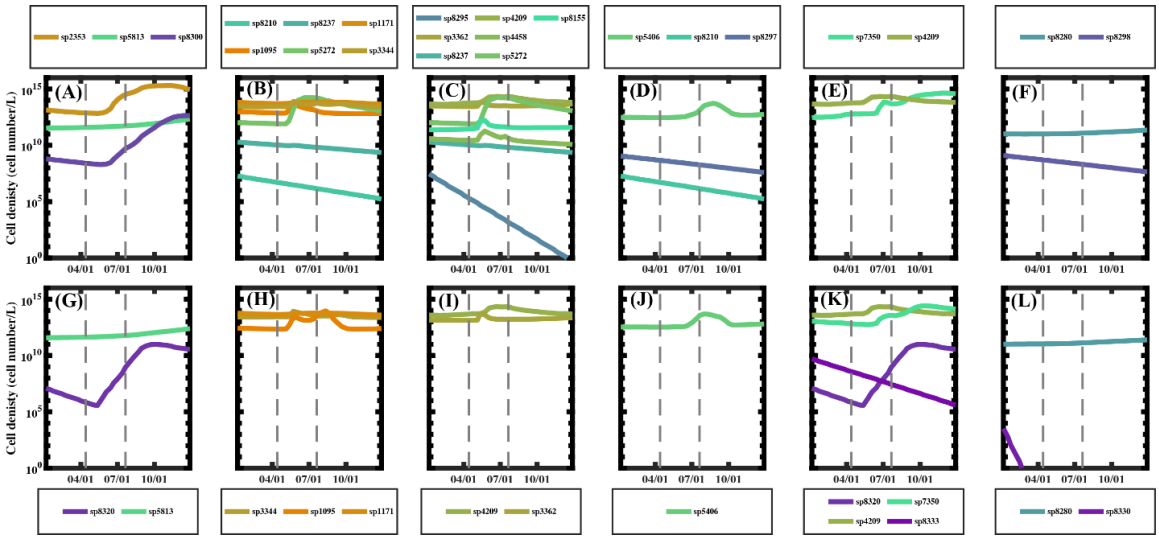

Fig. S2. The temporal responses of hydrocarbon degraders who are able to adapt to low temperature in the deep water. Cell density of different hydrocarbon degraders in the seep condition: (A) methane degraders, (B) ethane degraders, (C) propane degraders, (D) saturated degraders, (E) aromatic degraders, (F) resins degraders. Cell density of different hydrocarbon degraders in the no-seep condition: (G) methane degraders, (H) ethane degraders, (I) propane degraders, (J) saturated degraders, (K) aromatic degraders, (L) resins degraders. The two dashed grey lines represent the initiation and termination of the oil spill; different line colors represent different species, which are marked with a numeric ID from the predetermined microbial pool (e.g., sp2353).

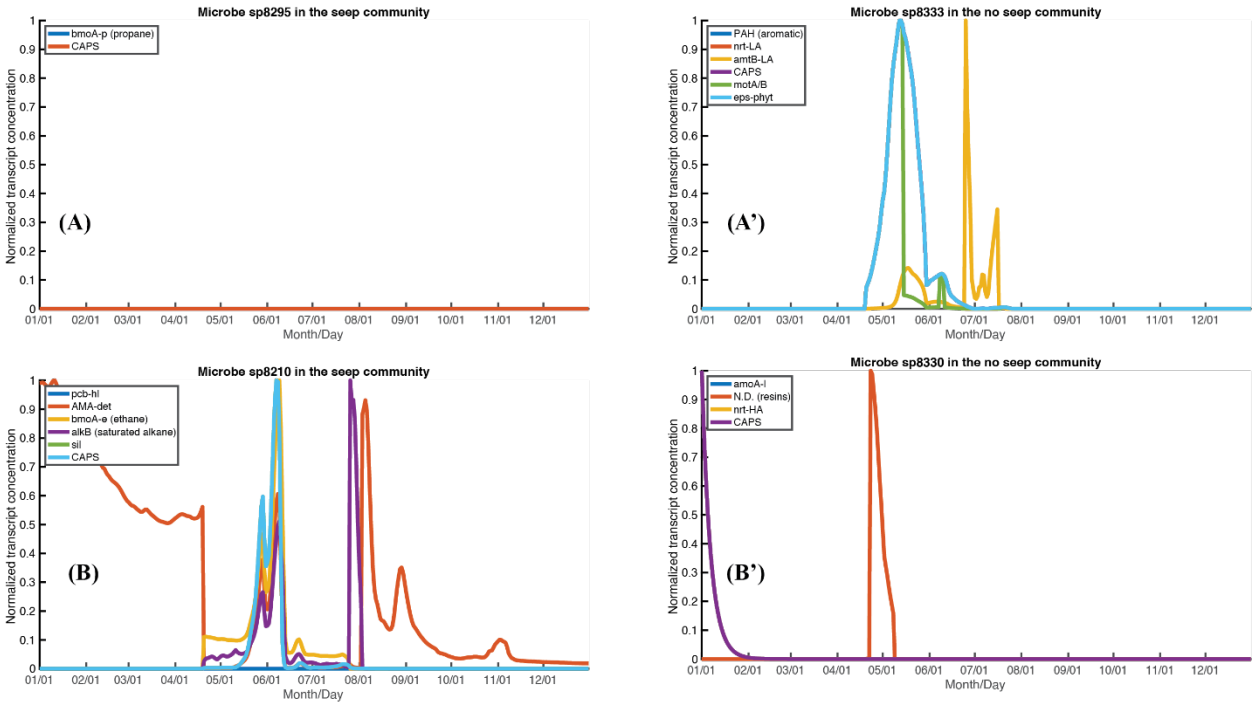

Fig. S3. Example of microbial effort from different low temperature adapted degraders in the plume layer at the blow-out site. Normalized transcript levels of all genes in different degraders: (A) sp8295 and (B) sp8210 in the seep condition, and (A') sp8333 and (B') sp8330 in the no-seep condition. Note: in the seep-adapted community, sp8297 has the same response as sp8295; and in the naïve community, sp8210 is the same as sp8237.

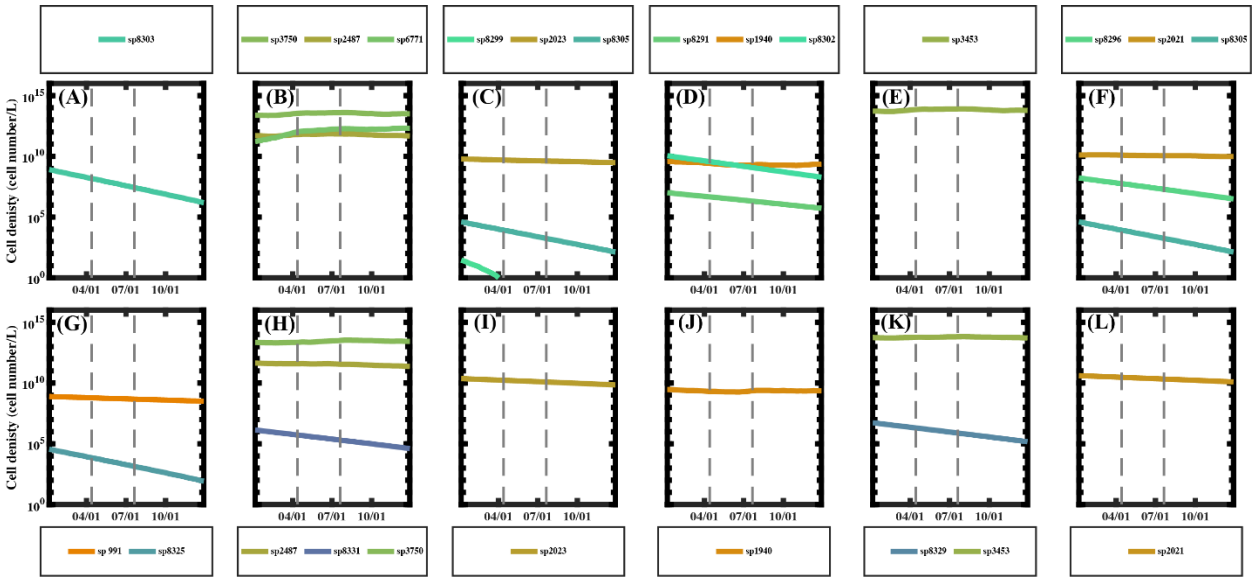

Fig.S4. The temporal responses of hydrocarbon degraders who are NOT able to adapt to low temperature in the deep water. Cell density of different hydrocarbon degraders in the seep condition: (A) methane degraders, (B) ethane degraders, (C) propane degraders, (D) saturated degraders, (E) aromatic degraders, (F) resins degraders. Cell density of different hydrocarbon degraders in the no-seep condition: (G) methane degraders, (H) ethane degraders, (I) propane degraders, (J) saturated degraders, (K) aromatic degraders, (L) resins degraders. The two dashed grey lines represent the initiation and termination of the oil spill; different line colors represent different species, which are marked with a numeric ID from the predetermined microbial pool (e.g., sp8303).

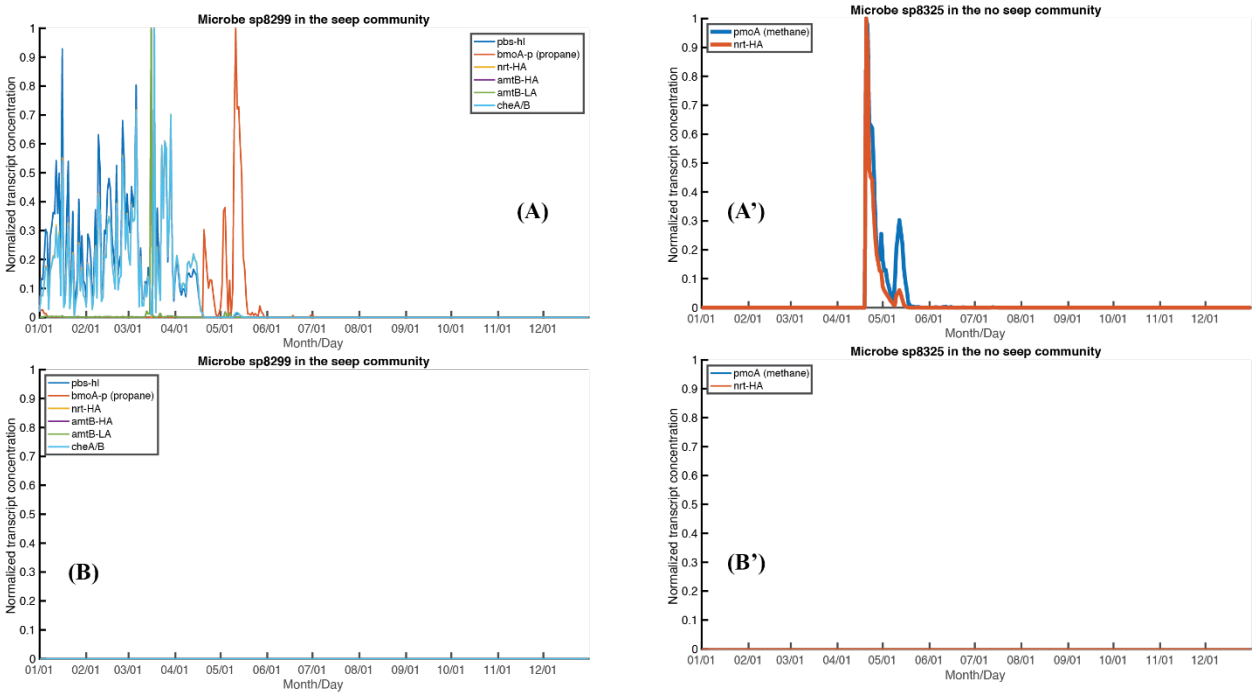

Fig.S5. Example of different microbial effort at surface water and deep water from degraders who are NOT able to adapt to low temperature at the blow-out site. Normalized transcript levels of all genes in degraders: sp8299 from the seep-adapted community in (A) the surface water and (B) the plume layer (deep water), and sp8325 from the naïve community in (A') the surface water and (B') the plume layer (deep water).

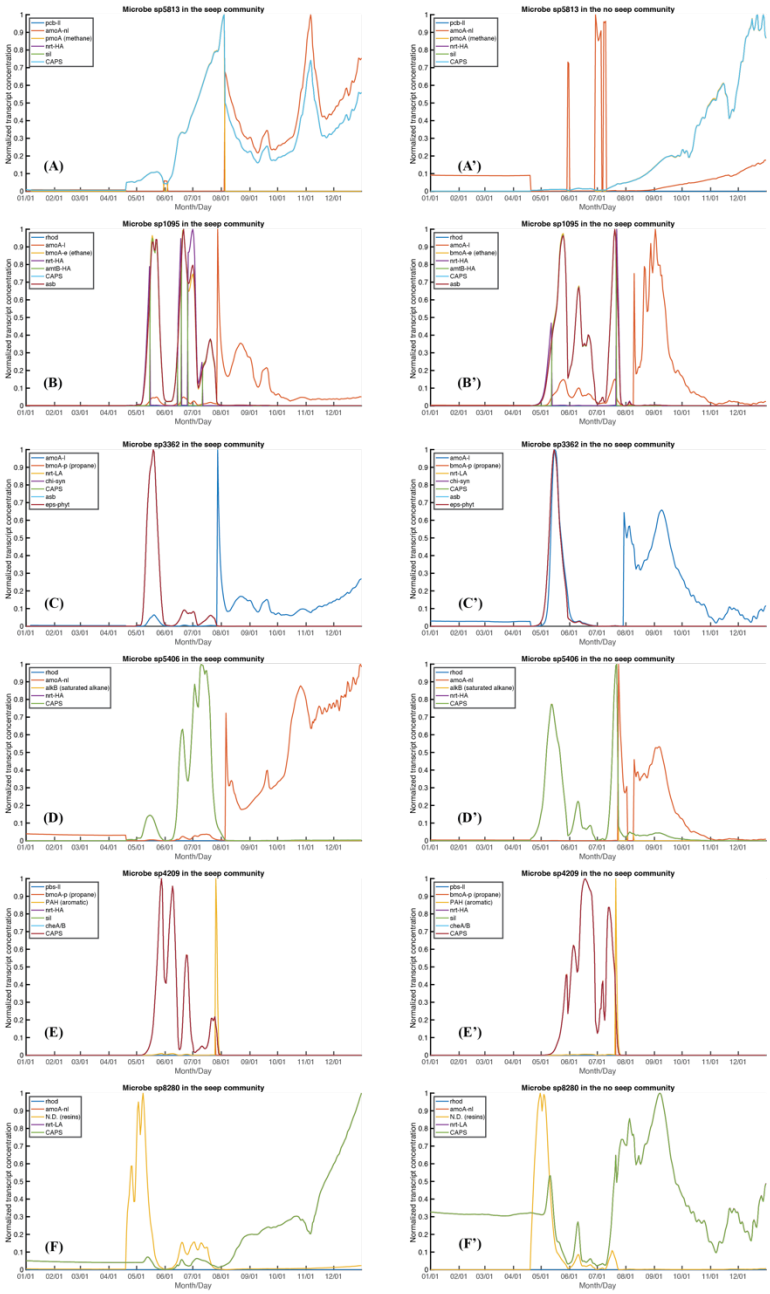

Fig. S6. Example of microbial effort from shared degraders existing in both emergent communities in the plume layer at the blow-out site. Temporal change of normalized transcript levels of selected hydrocarbon degraders: (A to F) hydrocarbon degraders in the seep-adapted community; (A' to F') hydrocarbon degraders in the naïve community. (A, A') sp5813, methane degrader; (B, B') sp1095, ethane degrader (C, C') sp3362, propane degrader; (D, D') sp5406, saturated hydrocarbon degrader; (E, E') sp4209, aromatic and propane degrader; (F, F') sp8280, resins degrader.

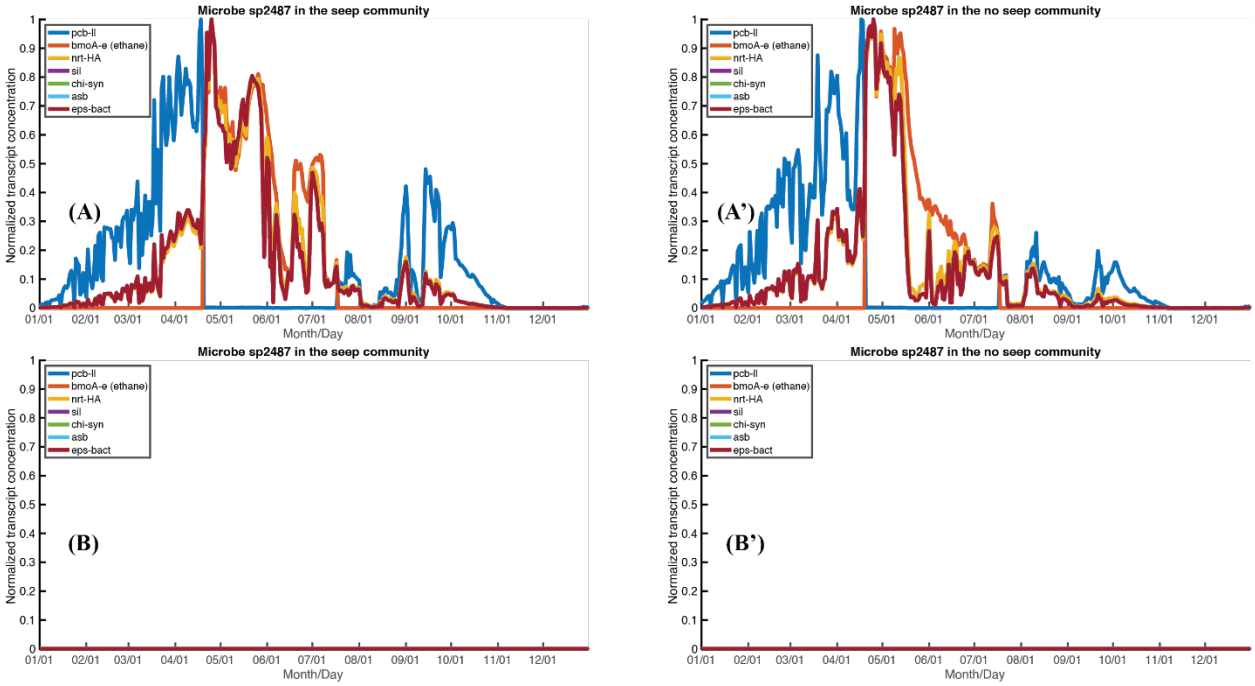

Fig.S7. Example of different microbial effort at surface water and deep water from shared degraders who emerge in both communities but are NOT able to adapt to low temperature at the blow-out site. Normalized transcript levels of all genes in degrader sp2487: temporal change at (A) the surface water and (B) the plume layer (deep water) in the seep condition, and temporal change at (A') the surface water and (B') the plume layer (deep water) in the no-seep condition.

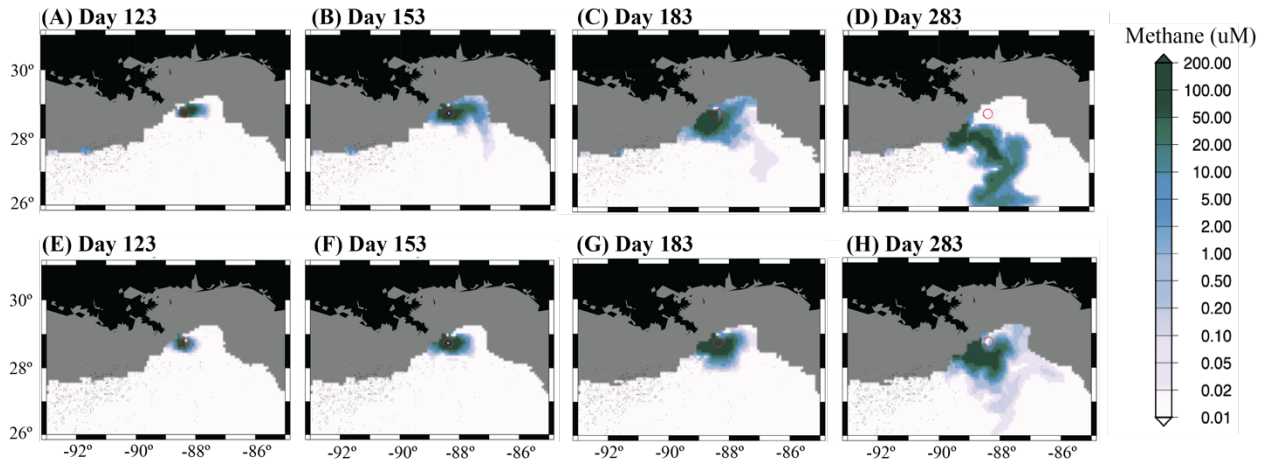

Fig.S8. Dissolved methane hydrocarbon concentration in the oil plume layer (~1000 - 1600m). (A-D) In the seep condition; (E-H) in the no-seep condition. The oil spill happened at day 110 of year 2010. (Red circle represents the well head location; dots represent field sampling sites after Valentine et al., 2010, and their color scale is the same as the map color scale. Only field samples taken within 10 days of the map date are depicted.

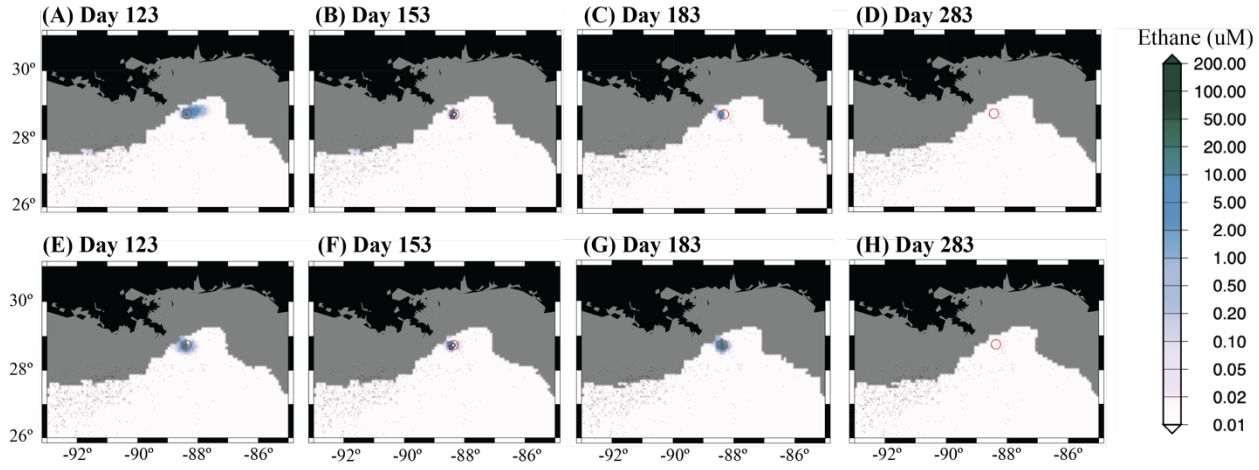

Fig.S9. Dissolved ethane hydrocarbon concentration in the oil plume layer (~1000 -1600m). **(A-D)** In the seep condition; **(E-H)** in the no-seep condition. The oil spill happened at day 110 of year 2010. (Red circle represents the well head location; dots represent field sampling sites after Valentine et al., 2010, and their color scale is the same as the map color scale. Only field samples taken within 10 days of the map date are depicted).

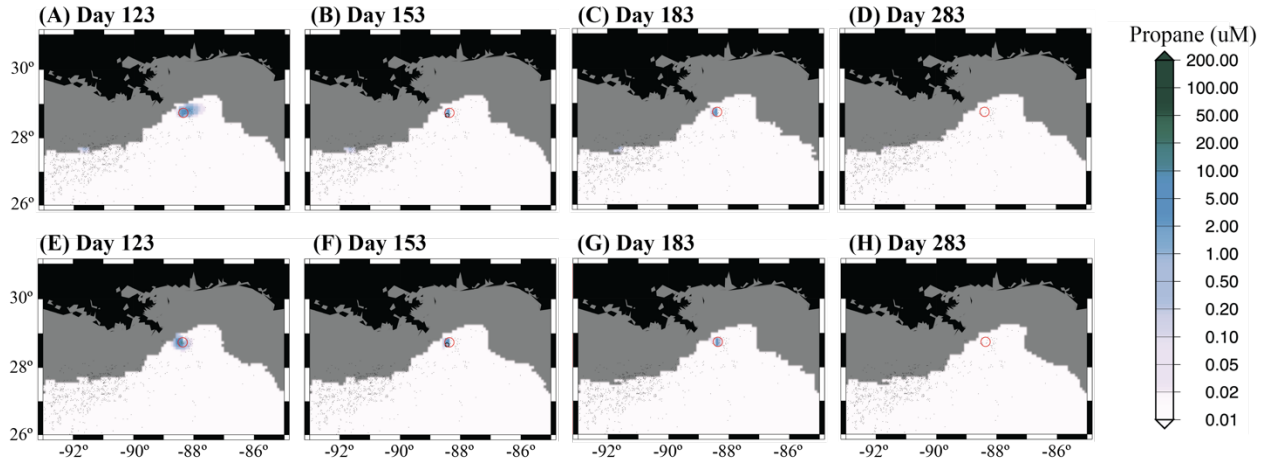

Fig.S10. Dissolved propane hydrocarbon concentration in the oil plume layer (~1000 - 1600m). (A-D) In the seep condition; (E-H) in the no-seep condition. The oil spill happened at day 110 of year 2010. (Red circle represents the well head location; dots represent field sampling sites after Valentine et al., 2010, and their color scale is the same as the map color scale. Only field samples taken within 10 days of the map date are depicted).

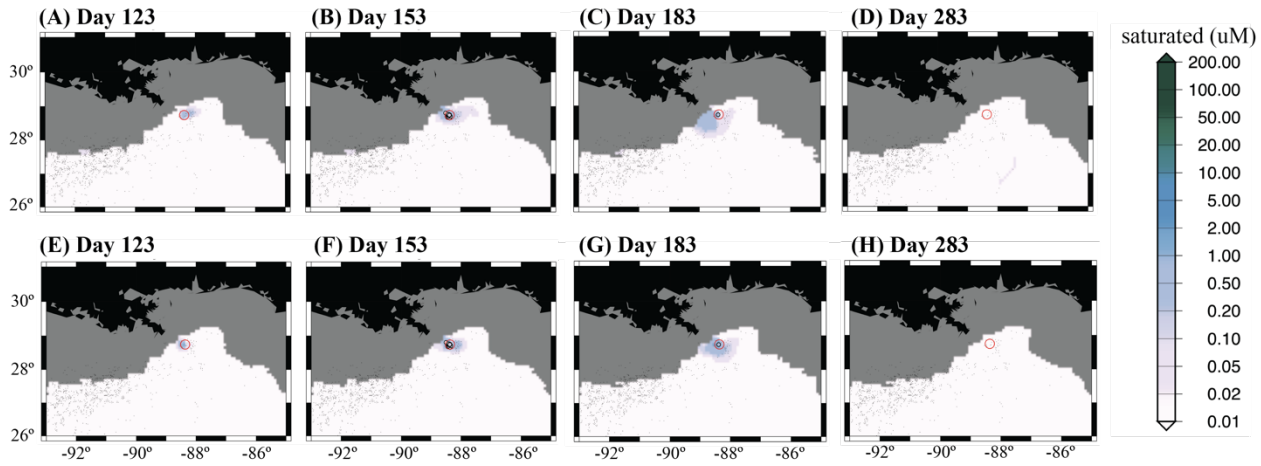

Fig. S11. Dissolved saturated hydrocarbon concentration in the oil plume layer (~1000 - 1600m). (A-D) In the seep condition; (E-H) in the no-seep condition. The oil spill happened at day 110 of year 2010. (Red circle represents the well head location; dots represent field sampling sites after Dubinsky et al. 2013, and their color scale is the same as the map color scale. Only field samples taken within 10 days of the map date are depicted).

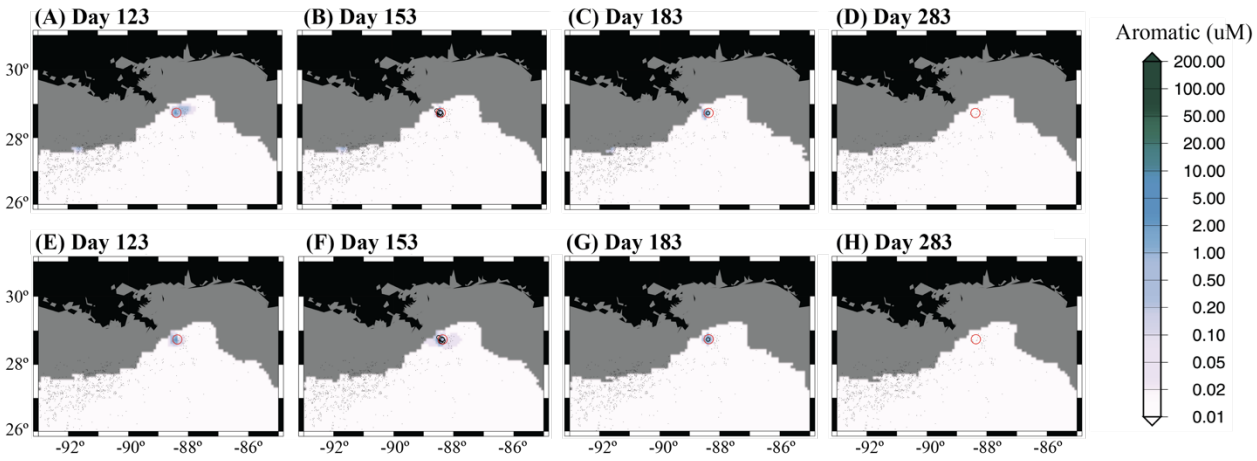

Fig.S12. Dissolved aromatic hydrocarbon concentration in the oil plume layer (~1000 - 1600m). (A-D) In the seep condition; (E-H) in the no-seep condition. The oil spill happened at day 110 of year 2010. (Red circle represents the well head location; dots represent field sampling sites after Dubinsky et al. 2013, and their color scale is the same as the map color scale. Only field samples taken within 10 days of the map date are depicted).

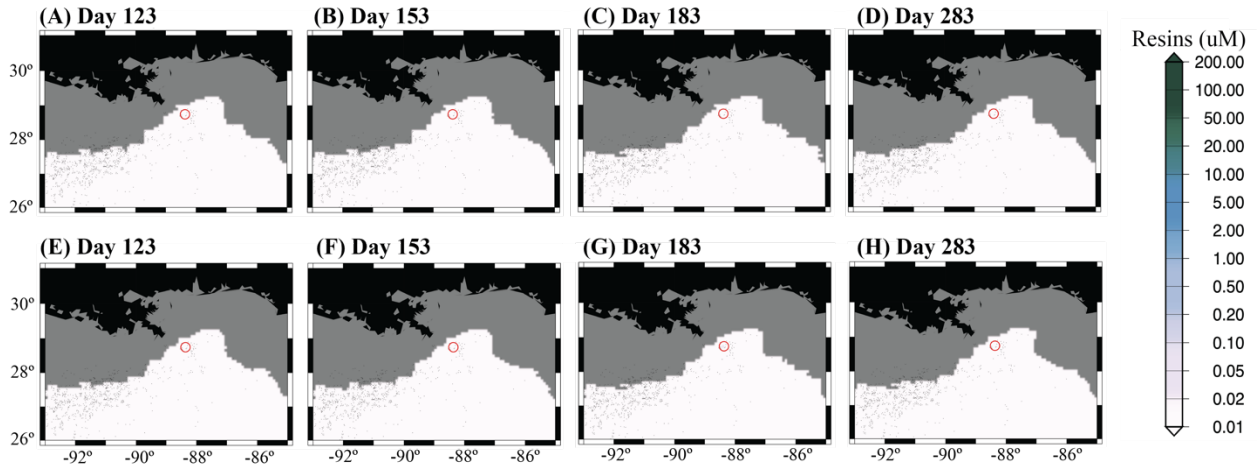

Fig.S13. Dissolved resin hydrocarbon concentration in the oil plume layer (~1000 -1600m). (A-D) In the seep condition; (E-H) in the no-seep condition. The oil spill happened at day 110 of year 2010. (Red circle represents the well head location).

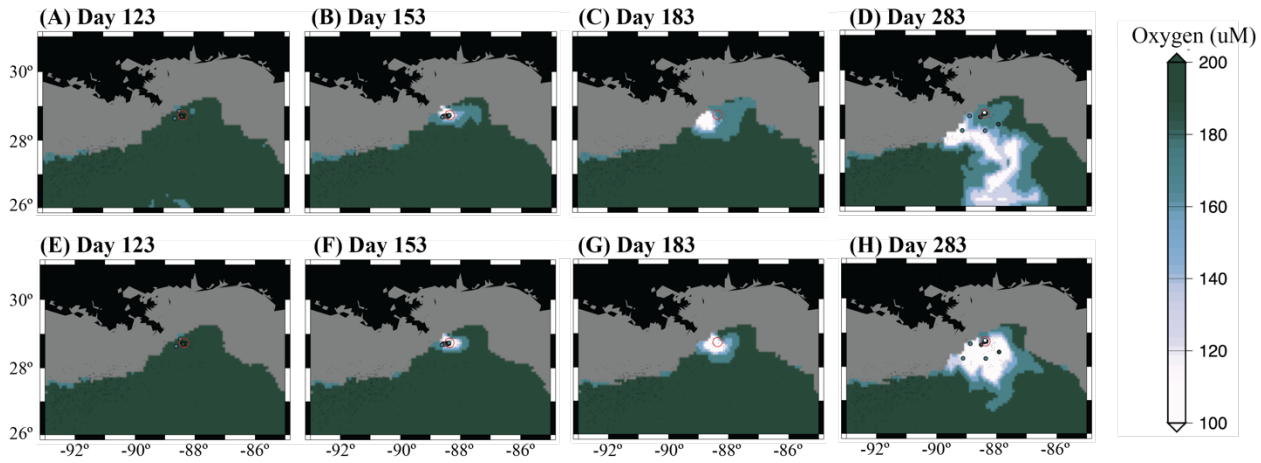

Fig.S14. Oxygen concentration in the oil plume layer (~1000 -1600m). (A-D) In the seep condition; (E-H) in the NO seep condition. The oil spill happened at day 110 of year 2010. (Red circle represents the well head location; dots represent field sampling sites after Shiller et al., 2012, and their color scale is the same as the map color scale. Only field samples taken within 10 days of the map date are depicted).

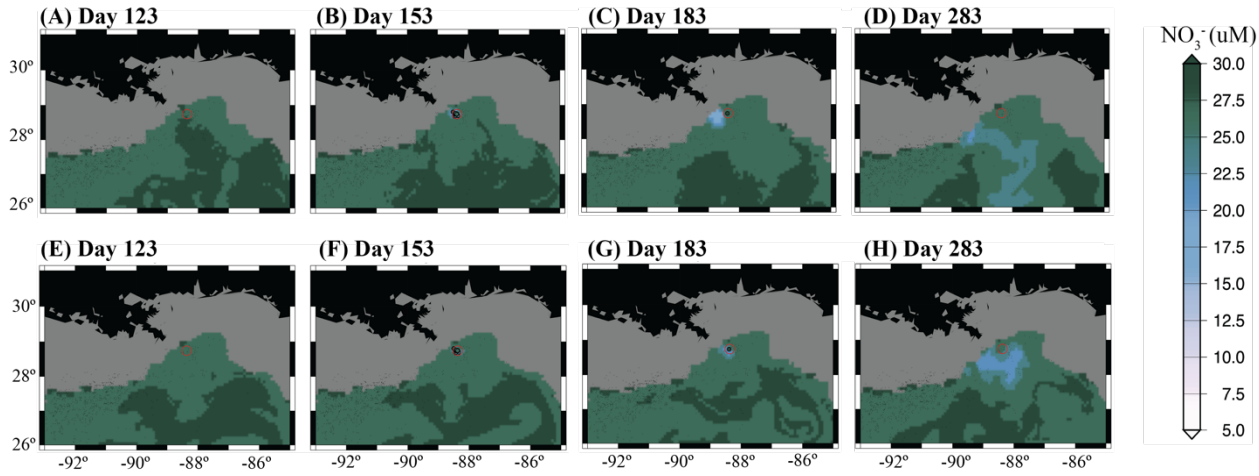

Fig.S15. Nitrate concentration in the oil plume layer (~1000 -1600m). (A-D) In the seep condition; (E-H) in the no-seep condition. The oil spill happened at day 110 of year 2010. (Red circle represents the well head location; dots represent field sampling sites after Shiller et al., 2012, and their color scale is the same as the map color scale. Only field samples taken within 10 days of the map date are depicted).

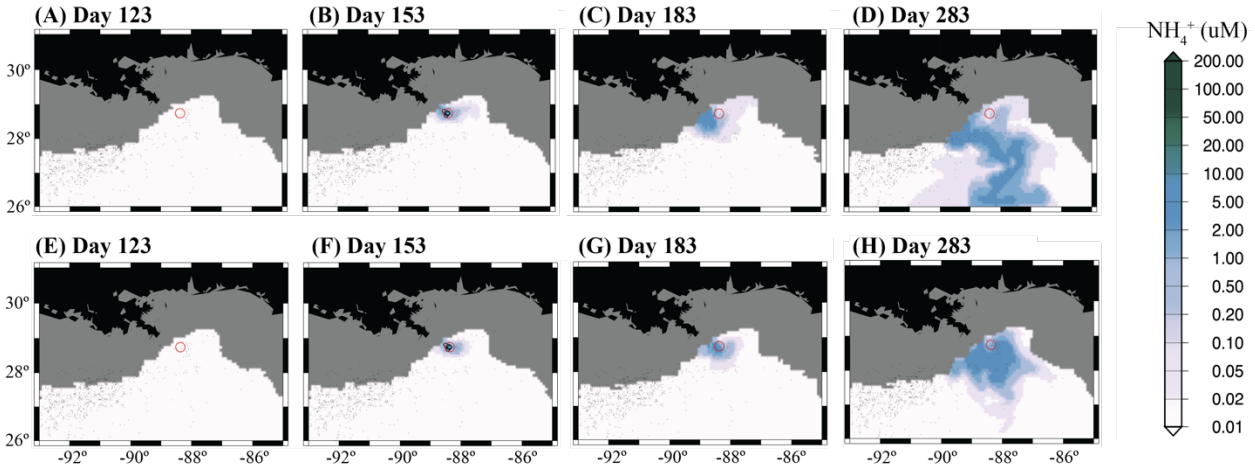

Fig.S16. Ammonium concentration in the oil plume layer (~1000 -1600m). (A-D) In the seep condition; (E-H) in the no-seep condition. The oil spill happened at day 110 of year 2010. (Red circle represents the well head location; dots represent field sampling sites after Dubinsky et al. 2013, and their color scale is the same as the map color scale. Only field samples taken within 10 days of the map date are depicted).

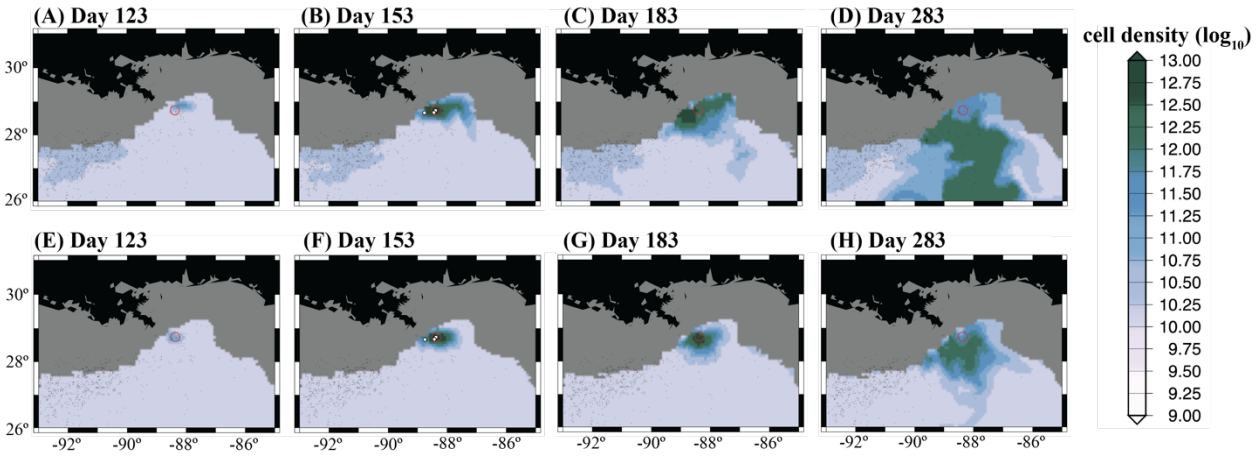

Fig.S17. The response of cell density (cells/L) to the spilled oil in the oil plume layer (~1000 -1600m). (A-D) In the seep condition; (E-H) in the no-seep condition. The oil spill happened at day 110 of year 2010. (Red circle represents the well head location; dots represent field sampling sites after Mason et al. 2012, and their color scale is the same as the map color scale. Only field samples taken within 10 days of the map date are depicted).

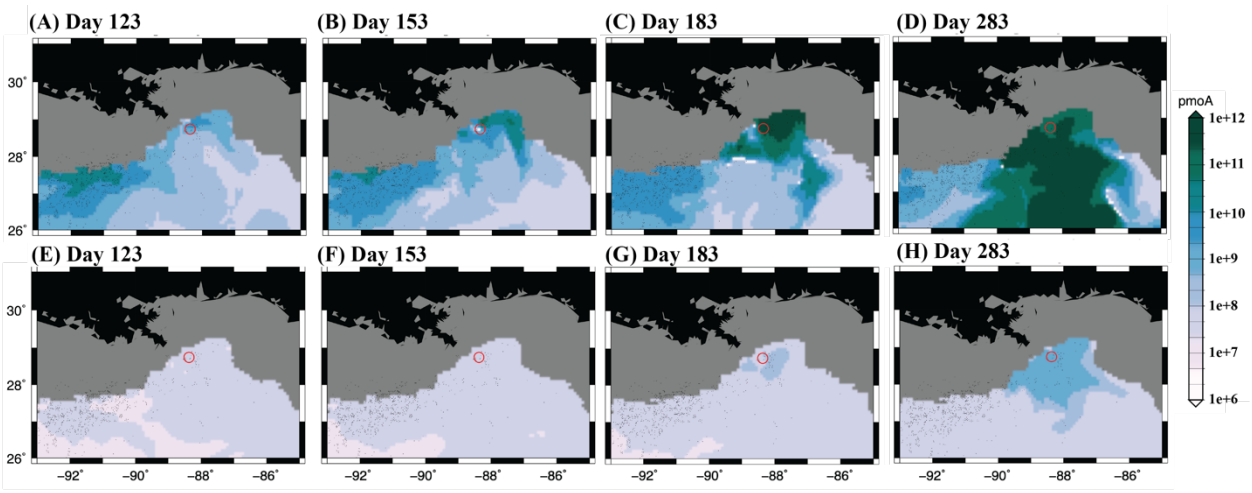

Fig.S18. The distribution of methane degrading gene pmoA (copies/L) in the oil plume layer (~1000 -1600m). (A-D) In the seep condition; (E-H) in the no-seep condition. the oil spill happened at day 110 of year 2010. (Red circle represents the well head location; small black dots are seep sites).

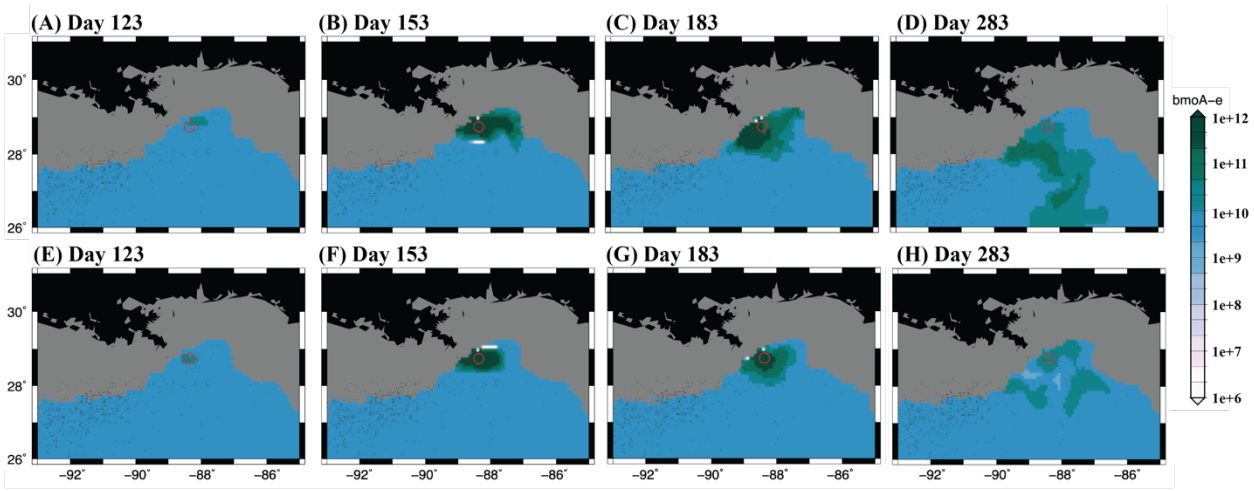

Fig.S19. The distribution of ethane degrading gene bmoA-e (copies/L) in the oil plume layer (~1000 -1600m). (A-D) In the seep condition; (E-H) in the no-seep condition. The oil spill happened at day 110 of year 2010. (Red circle represents the wellhead location; small black dots are seep sites).

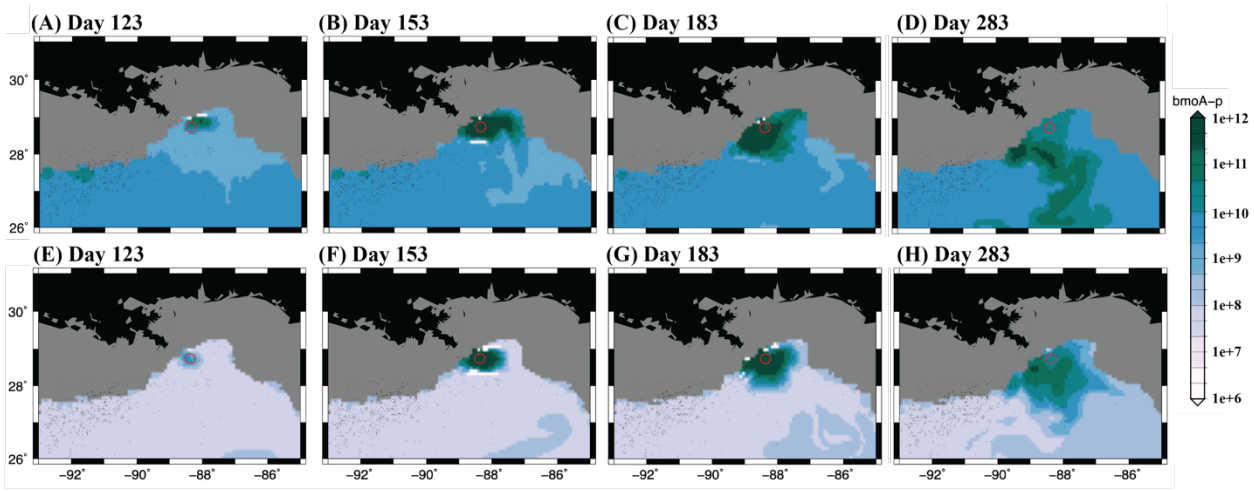

Fig.S20. The distribution of propane degrading gene bmoA-p (copies/L) in the oil plume layer (~1000 -1600m). (A-D) In the seep condition; (E-H) in the no-seep condition. The oil spill happened at day 110 of year 2010. (Red circle represents the well head location; small black dots are seep sites).

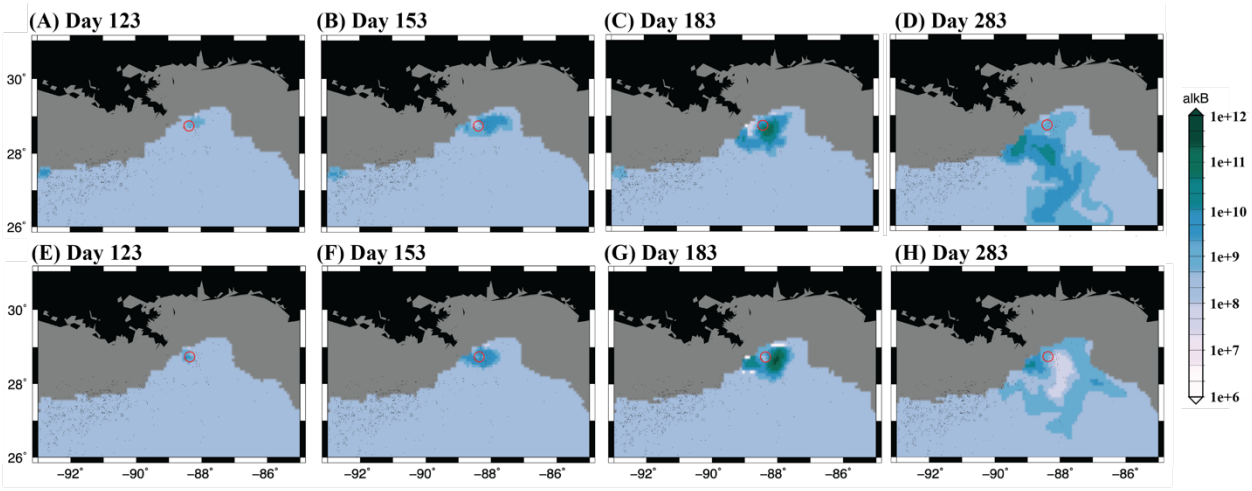

Fig.S21. The distribution of saturated hydrocarbon degrading gene alkB (copies/L) in the oil plume layer (~1000 -1600m). (A-D) In the seep condition; (E-H) in the no-seep condition. The oil spill happened at day 110 of year 2010. (Red circle represents the well head location; small black dots are seep sites).

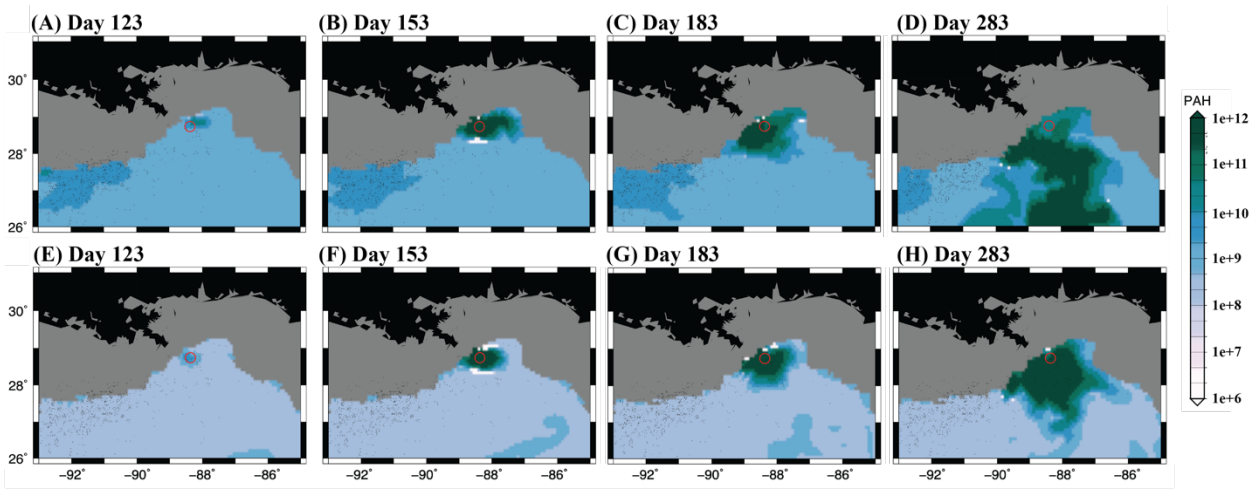

Fig.S22. The distribution of aromatic hydrocarbon degrading gene PAH (copies/L) in the oil plume layer (~1000 -1600m). (A-D) In the seep condition; (E-H) in the no-seep condition. The oil spill happened at day 110 of year 2010. (Red circle represents the well head location; small black dots are seep sites).

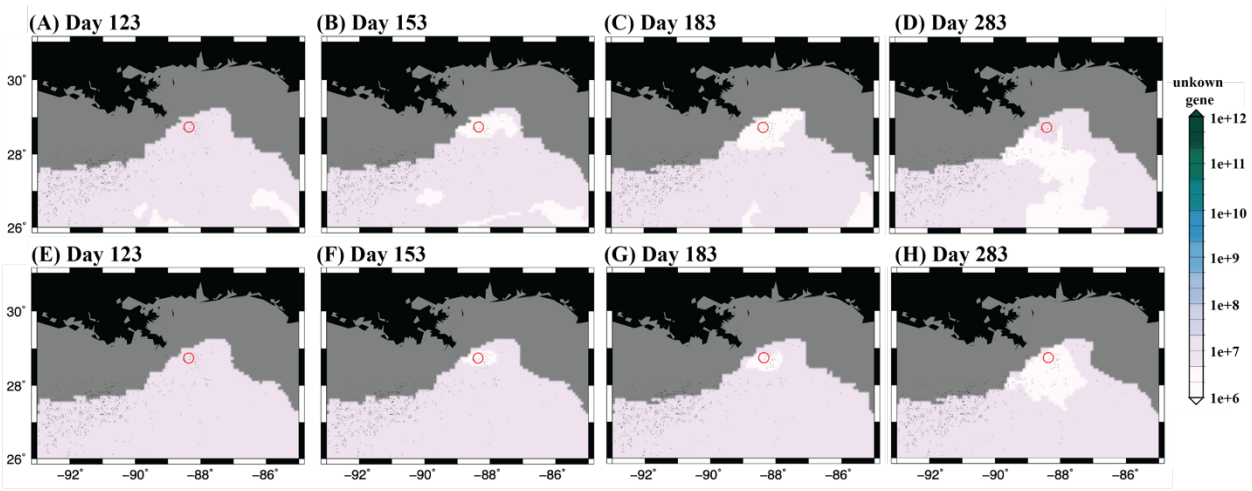

Fig.S23. The distribution of resins degrading gene (copies/L) in the oil plume layer (~1000 - 1600m). (A-D) In the seep condition; (E-H) in the no-seep condition. The oil spill happened at day 110 of year 2010. (Red circle represents the well head location; small black dots are seep sites).

Table S1.

The involvement level of species in hydrocarbon degradation under the two simulated conditions. Each community has a total of 58 species.

Hydrocarbon		Methane	Ethane	Propane	Saturated hydrocarbon	Aromatic hydrocarbon	Resins
Species involvement (%)	SEEP	7% (4/58)	16% (9/58)	36% (10/58)	10% (6/58)	5% (3/58)	9% (5/58)
	NO SEEP	7% (4/58)	10% (6/58)	5% (3/58)	3% (2/58)	10% (6/58)	5% (3/58)

Table S2.

Hydrocarbon half-lives calculated with two methods at the wellhead location. The method including physics is the one used in this study, and the other method normalizes other hydrocarbons with resins (19).

Half-life (days)	Methane	Ethane	Propane	Saturated	Aromatic	Resins	Method Ref.
Including physics	20.18	25.44	38.167	20.198	21.28	20.49	This study
Normalizing with resins	8.62	4.98	5.03	31.96	5.38	N.A.	(19)

Table S3.

Model gene names, functions and observed analogs. (N.D. means that no candidate comparison genes are known.)

Genes in the model	Gene function	Candidate comparison genes
pcb-hl	Light harvesting: low nutrient, high light adapted	psbA, pufL, pufM
pcb-ll	Light harvesting: low nutrient, low light adapted	psbA, pufL, pufM
pbs-hl	Light harvesting: non-specialist light harvest	psbA, pufL, pufM
pbs-ll	Light harvesting: non-specialist light harvest	psbA, pufL, pufM
rhod	Light harvesting: light driven proton pump	Bacteriorhodopsin, BchX, Proteorhodopsin
amoA-nl	Nitrification: bacterial nitrification without light inhibition	amoA
amoA-l	Nitrification: bacterial nitrification with light inhibition	amoA
pcaH	Heterotrophy: degradation of terrestrially derived organic matter	pcaH, vanA, Tannase, bglA
AMA	Heterotrophy: degradation of labile dissolved organic matter, e.g. amino acids	AA-Permease
pcaH-C	Heterotrophy: degradation of refractory dissolved organic carbon	pcaH, vanA, Tannase, bglA
AMA-C	Heterotrophy: degradation of labile dissolved organic carbon, e.g. amino acids	AA-Permease
AMA-det	Heterotrophy: degradation of labile particulate organic matter	AA-Permease
pmoA	Hydrocarbon degradation: allows degradation of gas hydrocarbons (e.g. methane)	pmoA
bmoA-e	Hydrocarbon degradation: allows degradation of gas hydrocarbons (e.g. ethane)	bmoA-e
bmoA-p	Hydrocarbon degradation: allows degradation of gas hydrocarbons (e.g. propane)	bmoA-p
alkB	Hydrocarbon degradation: allows degradation of hydrocarbons (e.g. saturated alkane)	alkB
PAH	Hydrocarbon degradation: allows degradation of hydrocarbons (e.g. aromatic hydrocarbon)	PAH
noGene	Hydrocarbon degradation: allows degradation of heavy hydrocarbons (e.g. resins)	N.D.
nif	Nitrogen Fixation: allows production of organic nitrogen from dissolved nitrogen gas	nifA, nifH
nrt-HA	Nutrient transport: high affinity transport and incorporation of nitrate	NAT, nrt ntrX, ntrY
nrt-LA	Nutrient transport: low affinity transport and incorporation of nitrate	NAT, nrt ntrX, ntrY
amtB-HA	Nutrient transport: high affinity transport and incorporation of ammonium	amtB, glnA
amtB-LA	Nutrient transport: low affinity transport and incorporation of ammonium	amtB
sil	Shell formation	
cheA/B	Protection: chemosensing to avoid predation	cheA, cheB, cheW
chi-syn	Buoyancy: formation of features that reduce sinking (e.g. chitin synthase)	Chs3p
CAPs	Low temperature adaptation (e.g. psychrophile)	CAPs
asb	abc transporters	N.D.
motA/B	Motility: for particle Attachment	motA, motB
eps-phytoplankton	Exude polysaccharides under light stress	N.D.
eps-bacteria	Exude polysaccharides under nutrient stress	N.D.

Table S4.

Mass flux of hydrocarbons from the Deepwater Horizon (DwH) Oill Spill in the GENOME model.

Group		Methane		Ethane		Propane		Saturated	Aromatic	Resins
Typical formula		CH_4		C_2H_6		C_3H_8		$C_{10}H_{22}$	C_7H_8	$C_{30}H_{52}$
Mass rate (g/s)	Surface water	34056.78	340.56	3152.68	252.21	1712.56	359.63	9435.10	2040.02	1275.01
	Deep water		33716.21		2900.46		1352.92	24030.65	5195.81	3247.38
Ref.		(6, 25–27)								

Table S5.

Seep hydrocarbon composition and mass flux in the GENOME model.

Group	Methane	Ethane	Propane	Saturated	Aromatic	Resins
Typical formula	CH_4	C_2H_6	C_3H_8	$C_{10}H_{22}$	C_7H_8	$C_{30}H_{52}$
Total seepage site	938					
Total mass rate (g/s)	4439.36					
Mass fraction	0.5356	0.0399	0.0943	0.0748	0.1988	0.0566
Typical mass rate (g/s)	2377.7212	177.1305	418.6316	332.0641	882.5448	251.2678
Ref.	(28–33)					

SI References

1. S. W. Myint, N. D. Walker, Quantification of surface suspended sediments along a river dominated coast with NOAA AVHRR and Sea WiFS measurements: Louisiana, USA. *Int. J. Remote Sens.* **23**, 3229–3249 (2002).
2. G. A. Snedden, J. E. Cable, C. Swarzenski, E. Swenson, Sediment discharge into a subsiding Louisiana deltaic estuary through a Mississippi River diversion. *Estuar. Coast. Shelf Sci.* **71**, 181–193 (2007).
3. J. Wang, K. Xu, C. Li, J. B. Obelcz, Forces driving the morphological evolution of a mud-capped dredge pit, northern Gulf of Mexico. *Water (Switzerland)* **10** (2018).
4. D. López-Veneroni, L. A. Cifuentes, Transport of dissolved organic nitrogen in Mississippi River plume and Texas-Louisiana continental shelf near-surface waters. *Estuaries* **17**, 796–808 (1994).
5. S. Saha, *et al.*, The NCEP climate forecast system reanalysis. *Bull. Am. Meteorol. Soc.* **91**, 1015–1057 (2010).
6. O. U. Mason, *et al.*, Metagenome, metatranscriptome and single-cell sequencing reveal microbial response to Deepwater Horizon oil spill. *ISME J.* **6**, 1715–1727 (2012).
7. V. J. Coles, *et al.*, Ocean biogeochemistry modeled with emergent trait-based genomics. *Science (80-.).* **358**, 1149–1154 (2017).
8. E. E. Roden, Q. Jin, Thermodynamics of microbial growth coupled to metabolism of glucose, ethanol, short-chain organic acids, and hydrogen. *Appl. Environ. Microbiol.* **77**, 1907–1909 (2011).
9. J. A. Roels, the Application of Macroscopic Principles To Microbial Metabolism. *Ann. N. Y. Acad. Sci.* **369**, 113–134 (1981).
10. P. G. Verity, *et al.*, Relationships between cell volume and the carbon and nitrogen content of marine photosynthetic nanoplankton. *Limnol. Oceanogr.* **37**, 1434–1446 (1992).
11. B. Cho, F. Azam, Biogeochemical significance of bacterial biomass in the ocean's euphotic zone. *Mar. Ecol. Prog. Ser.* **63**, 253–259 (1990).
12. S. Menden-Deuer, E. J. Lessard, Carbon to volume relationships for dinoflagellates, diatoms, and other protist plankton. *Limnol. Oceanogr.* **45**, 569–579 (2000).
13. U. Sommer, *et al.*, Beyond the plankton ecology group (PEG) model: Mechanisms driving plankton succession. *Annu. Rev. Ecol. Evol. Syst.* **43**, 429–448 (2012).
14. S. L.Pimm, The complexity and stability of ecosystems. *Nature* **315**, 635–636 (1985).
15. A. Shade, *et al.*, Fundamentals of microbial community resistance and resilience. *Front. Microbiol.* **3**, 1–19 (2012).
16. K. N. Suding, K. L. Gross, G. R. Houseman, Alternative states and positive feedbacks in restoration ecology. *Trends Ecol. Evol.* **19**, 46–53 (2004).
17. D. A. Orwin, K.H., Wardle, New indices for quantifying the resistance and resilience of soil biota to exogenous disturbances. *Soil Biol. Biochem.* **36**, 1907–1912 (2004).
18. W. E. Westman, Measuring the Inertia and Resilience of Ecosystems. *Bioscience* **28**, 705–710 (1978).
19. A. E. Thessen, E. W. North, Calculating in situ degradation rates of hydrocarbon compounds in deep waters of the Gulf of Mexico. *Mar. Pollut. Bull.* **122**, 77–84 (2017).
20. M. A. Zahed, *et al.*, Kinetic modeling and half life study on bioremediation of crude oil dispersed by Corexit 9500. *J. Hazard. Mater.* **185**, 1027–1031 (2011).
21. S. E. Agarry, M. O. Aremu, O. A. Aworanti, Biodegradation of 2,6-Dichlorophenol Wastewater in Soil Column Reactor in the Presence of Pineapple Peels-Derived Activated Carbon, Palm Kernel Oil and Inorganic Fertilizer. *J. Environ. Prot. (Irvine,. Calif).* **04**, 537–547 (2013).
22. D. L. Valentine, *et al.*, Dynamic autoinoculation and the microbial ecology of a deep water hydrocarbon irruption. *Proc. Natl. Acad. Sci. U. S. A.* **109**, 20286–20291 (2012).
23. E. A. Dubinsky, *et al.*, Succession of hydrocarbon-degrading bacteria in the aftermath of the deepwater horizon oil spill in the gulf of Mexico. *Environ. Sci. Technol.* **47**, 10860–10867 (2013).
24. A. M. Shiller, D. Joung, Nutrient depletion as a proxy for microbial growth in Deepwater Horizon subsurface oil/gas plumes. *Environ. Res. Lett.* **7** (2012).
25. D. L. Valentine, *et al.*, Propane respiration jump-starts microbial response to a deep oil

spill. *Science (80-.).* **330**, 208–211 (2010).
26. A. R. Diercks, *et al.*, Characterization of subsurface polycyclic aromatic hydrocarbons at the Deepwater Horizon site. *Geophys. Res. Lett.* **37**, 1–6 (2010).
27. C. M. Reddy, *et al.*, Composition and fate of gas and oil released to the water column during the Deepwater Horizon oil spill. *Proc. Natl. Acad. Sci.* **109**, 20229 LP – 20234 (2012).
28. I. R. MacDonald, *et al.*, Natural and unnatural oil slicks in the Gulf of Mexico. *J. Geophys. Res. Ocean.* **120**, 8364–8380 (2015).
29. H. C. (ed. . Ward, *Water quality of the Gulf of Mexico* (2017).
30. Coleman, J., Baker, C., Cooper, C.K., Fingas, M., Hunt, G., Kvenvolden, K.A., Michel, K., Michel, J., R. B. McDowell, J., Phinney, P., Rabalais, N., Roesner, L., Spies, *Oil in the Sea III* (The National Academies Press, 2003) https:/doi.org/10.17226/10388.
31. L. M. Sauer, T.C., Jr., Sackett, W.M. and Jeffrey, Volatile liquid hydrocarbons in the surface coastal waters of the Gulf of Mexico. *Mar. Chem.* **7**, 1–16 (1978).
32. T. L. Wade, M. C. Kennicutt, J. M. Brooks, Gulf of Mexico Hydrocarbon Seep Communities: Part III. Aromatic Hydrocarbon Concentrations in Organisms, Sediments and Water. *Mar. Environ. Res.* **27**, 19–30 (1989).
33. T. Mitra, Siddhartha, Bianchi, A preliminary assessment of polycyclic aromatic hydrocarbon distributions in the lower Mississippi River and Gulf of Mexico. *Mar. Chem.* **82**, 273–288 (2003).